Journal of Sound and Vibration 541 (2022) 117279

Contents lists available at ScienceDirect

Journal of Sound and Vibration

journal homepage: www.elsevier.com/locate/jsvi

A unified framework for acoustic instabilities based on the tailored Green's function

Maria A. Heckl [a,*], Sreenath Malamal Gopinathan [a], Aswathy Surendran [a,b]

[a] School of Chemical and Physical Sciences, Keele University, Staffordshire ST5 5BG, UK
[b] Professur für Thermofluiddynamik, Technische Universität München, 85747 Garching, Germany

ARTICLE INFO

Keywords:
Tailored Green's function
Volterra integral equation
Duct acoustics
Instability
Monopole
Dipole

ABSTRACT

This paper presents a unified framework to analyse the role of thermoacoustic and aeroacoustic sources in a one-dimensional acoustic resonator. We introduce two forms of the tailored Green's function: one that satisfies the boundary conditions of the acoustic pressure and one that satisfies those of the acoustic velocity. We consider acoustic sources, which can enter into a feedback loop with the acoustic field in the resonator and hence give rise to an instability. We assume that they are compact, and we model them as a monopole, dipole or a combination of the two. The reaction of a source to the acoustic field can be described in the time-domain (e.g. by a relationship between the volume outflow of a monopole to the local acoustic velocity at earlier times) or in the frequency domain (e.g. by a transfer matrix). Governing equations for the complete acoustic system are derived from the 1-D version of the acoustic analogy equation, using a Green's function approach. They turn out to be two coupled Volterra equations for the acoustic pressure and velocity. Their solution is straightforward and numerically inexpensive. We demonstrate our approach with three diverse examples: a nonlinear Rijke tube, a whistling orifice, and a flame anchored on an orifice plate with bias flow. Our framework can be applied to various configurations, in particular to combustion test rigs, which consist of a duct-shaped resonator housing acoustically active elements, such as a flame and an orifice with bias flow.

Preamble by Maria Heckl

This article is in memory of Professor Shôn Ffowcs Williams, who was my PhD supervisor in the 1980s and had a lasting positive influence on my career. Shôn's guidance was both stimulating and hands-off, and he encouraged me early on to become an independent researcher. When I had finished my PhD, Shôn secured funding from the then UK Atomic Energy Authority (UKAEA) for a post-doctoral position. My task was to develop a new acoustic monitoring method that he called the "Green's function calibration scheme". I accepted the position, not knowing what he meant by that and assuming that my sponsors at the UKAEA would enlighten me. It turned out in my first meeting with them that they did not know either and that Shôn had sold them a pig in a poke. The way forward for me was to get to grips with Green's function techniques used in acoustics. This lead not only to a very fruitful collaboration between UKAEA and me, but it developed in me a deep appreciation of the Green's function, and this has served me very well throughout my career. My two co-authors are from the next generation of Shôn's academic offspring: Sreenath Malamal Gopinathan is a former post-doc of mine, and Aswathy Surendran is a former PhD student.

* Corresponding author.
E-mail address: m.a.heckl@keele.ac.uk (M.A. Heckl).

https://doi.org/10.1016/j.jsv.2022.117279
Received 15 January 2022; Received in revised form 31 August 2022; Accepted 31 August 2022
Available online 7 September 2022

List of symbols

a_k, b_k	fitting parameters for approximation by rational functions
B	abbreviation for $(\gamma-1)\bar{\rho}/c^2$
c	speed of sound
D_o	orifice diameter
F	global force
f	local force distribution
i	imaginary unit
L	length of 1-D cavity
n	mode number
n_0, n_1	coupling coefficients
p	pressure
Q	global heat release rate
q	local heat release rate (per unit mass)
R_0, R_L	reflection coefficients
Re	Reynolds number
St	Strouhal number
$s(\mathbf{x},t)$	acoustic source distribution
T_{11}, T_{12}, T_{21}, T_{22}	elements of the transfer matrix
$\bar{T}$	mean temperature
T_1, T_2	time periods of modes 1 and 2
$\mathcal{T}(\omega)$	flame transfer function
t	observer time
t^*	source time
t_o	thickness of orifice plate
u	velocity
$\bar{u}_o$	bias flow velocity
$\mathbf{x}=(x_1,x_2,x_3)$, x	observer position (3-D and 1-D)
$\mathbf{x}^*$, x^*	position of the hypothetical point source occurring in the Greens function
x_q	axial coordinate of source position
V	volume
$Z(\omega)$	transfer impedance
γ	specific heat ratio
ν	kinematic viscosity
ρ	mass density
τ	time-lag
ω	angular frequency
G	Green's function
$H(x)$	Heaviside function
δ	delta function

Overbars denote the mean part of field quantities, primes denote the fluctuating part of field quantities in the time-domain, and hats denote the fluctuating part of field quantities in the frequency-domain. For example, for the global heat release rate, $Q(t)=\bar{Q}+Q'(t)$, where $\bar{Q}$ is the mean part, and $Q'(t)$ and $\hat{Q}(\omega)$ are, respectively, the fluctuating part in the time domain and frequency domain. The starred symbols x^*, t^* denote source position and source time. The time dependence of a quantity oscillating with frequency ω is denoted by $\mathrm{e}^{-\mathrm{i}\omega t}$.

1. Introduction

The Green's function is an impulse response. It has not only a clear physical meaning in that it can be measured, but it is also a very useful mathematical tool for solving linear partial differential equations with a nonhomogeneity acting as the source term (see chapter 2 by Ffowcs Williams in [1]). Green's functions are named after the mathematician George Green, who was the first to develop the concept in the 1820s [2] and applied it to electrostatic problems. Green's functions were subsequently used to solve other partial differential equations (PDEs) governing a variety of physical phenomena.

The use of Green's functions in acoustics took off with the emergence of Lighthill's theory [3,4]. By reformulating the compressible Navier–Stokes equations, Lighthill derived his famous acoustic analogy equation, which is a nonhomogeneous wave equation for the acoustic field. This equation, he then turned into an integral equation with the help of the Green's function. The integral formulation proved to be very convenient for understanding the noise generation mechanisms due to aeroacoustic and thermoacoustic processes; it also provided a suitable framework for introducing approximations [5,6].

In acoustics, the Green's functions are the solution of the special nonhomogeneous wave equation

$$\frac{1}{c^2}\frac{\partial^2 G}{\partial t^2} - \frac{\partial^2 G}{\partial x_i^2} = \delta\left(\mathbf{x}-\mathbf{x}^*\right)\ \delta\left(t-t^*\right)\ , \tag{1.1}$$

where δ denotes the delta function, and $\partial^2/\partial x_i^2$ is the Laplace operator. The Green's function represents the sound field generated by a point source at position $\mathbf{x}^*$, firing an impulse at time t^*, and observed by a listener at position $\mathbf{x}$ and time by t. We denote it by

$$G = G\left(\mathbf{x}, t; \mathbf{x}^*, t^*\right)\ . \tag{1.2}$$

G satisfies the causality condition that no sound can be observed *before* the impulse has been fired, i.e.

$$G = 0 \qquad \text{and} \qquad \frac{\partial G}{\partial t} = 0 \quad \text{for} \quad t \le t^*\ . \tag{1.3}$$

In unbounded space, the solution of Eq. (1.1) that satisfies Eq. (1.3) is known analytically, and given by

$$G\left(\mathbf{x}, t; \mathbf{x}^*, t^*\right) = \frac{\delta\left[(t-t^*) - |\mathbf{x}-\mathbf{x}^*|/c\right]}{4\pi\,|\mathbf{x}-\mathbf{x}^*|}\ ; \tag{1.4}$$

this is called the "free-space Green's function". It is widely used in acoustics, in particular to predict aerodynamic sound in unbounded flows.

If the impulsive point source acts in a space with boundaries, the resulting acoustic field adapts to these boundaries and is generally quite different from the response in the free field. The Green's function, which satisfies the relevant boundary conditions is called the "exact Green's function" or the "tailored Green's function", because it is tailored to the relevant geometry. Doak [7] was the first to use tailored Green's functions in conjunction with Lighthill's acoustic analogy equation.

The tailored Green's function is an under-used mathematical tool in fundamental studies of self-excited acoustic oscillations. Yet it offers an elegant framework to study oscillations driven by thermoacoustic and/or aeroacoustic feedback. The purpose of this paper is to advocate this framework and to illustrate its advantages with suitable examples.

The tailored Green's function is known in analytical form only for a limited number of elementary geometries. Three-dimensional space with a thin rigid half-plane is one such geometry. It has been applied by various aeroacoustics researchers to study the noise from the edge of an aerofoil. Ffowcs Williams and Hall [8] used it to model noise generation by a half-plane in turbulent fluid. Howe [9] extended the approach to small acoustic frequencies. Roger [10] used this tailored Green's function to predict the tonal noise of distributed propellers installed above the wing of an aircraft.

A far-field approximation of the tailored Green's function was developed by Howe [11]. This is known as the "compact Green's function" or "low-frequency Green's function", and is valid for the special case where the source is close to a compact object (scatterer) and the observer is far from the source. It has been applied successfully to model a variety of sound generation scenarios, for example

- the sound generated when a density inhomogeneity is swept out of a nozzle into free space [12]
- the compression wave produced when a high-speed train enters a tunnel [13]
- the sound produced by unsteady throttling of flow into a resonant cavity with application to voiced speech [14].

Another class of the tailored Green's function is the enclosed-space Green's function. This represents the interior sound field generated by a point source in a *cavity* and is a superposition of cavity modes. Analytical representations are known for simple geometries, for example ducts of finite length, rectangular, cylindrical and annular cavities (see, for example, [15], chapter 7; [16], chapters 7 and 9). Applications are quite uncommon, but a few scenarios have been modelled:

- Doak [17,18] described the acoustic field generated by a distribution of wall-mounted pistons in a finite-length rigid duct.
- Kang and Kim [19] determined the acoustic field in a finite three-port cylindrical chamber with variable end conditions.
- Veerababu and Venkatesham [20] calculated the transmission loss of a concentric tube resonator.

The tailored Green's function for a cavity is usually represented by a sum of eigenmodes (see [15], section 7.1). This representation has poor convergence, which stems from the fact that the Green's function has a singularity where the source and observer position coincide, whereas the eigenfunctions are analytical throughout. An alternative representation, which has a built-in singularity, has been developed by Heckl and Howe [21]. They consider a piecewise uniform 1-D duct with a localised jump in cross-section and in mean temperature. The source position is assumed to be close to the jump, while the observer position can be anywhere on either side of the jump. Heckl and Howe expressed the Green's function as two separate functions, corresponding to the two separate sections of the piecewise duct. One function satisfies the upstream boundary condition and is valid for observers in the upstream section, while the other function satisfies the downstream boundary condition and is valid for the downstream section. They use generalised functions to calculate the Green's function in the frequency-domain and then apply a Fourier transform to get the time-domain version. Their result is a superposition of "modes", which are similar to the duct modes in that they have the same frequencies; however, they differ from the duct modes in that they have a singularity at the source position.

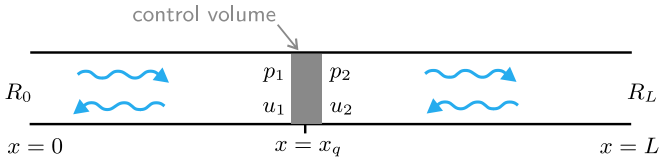

Fig. 1. Finite duct with a source enclosed by a compact control volume.

Acoustic waves generated by a source distribution $s(\mathbf{x}, t)$ are described by the nonhomogeneous wave equation, e.g. for the pressure p'

$$\frac{1}{c^2}\frac{\partial^2 p'}{\partial t^2} - \frac{\partial^2 p'}{\partial x_i^2} = s(\mathbf{x}, t)\,. \tag{1.5}$$

This equation can be written with Eq. (1.1) in integral form

$$p'(\mathbf{x}, t) = \int_{t^*=0}^{t} \int_V s(\mathbf{x}^*, t^*)\, G\left(\mathbf{x}, t; \mathbf{x}^*, t^*\right) \mathrm{d}V^*\, \mathrm{d}t^* \;+\; \text{b.c.}\,, \tag{1.6}$$

where V is a control volume that encloses the sources, and b.c. abbreviates a term, which involves a surface integral over the boundary of V. This term is zero if the tailored Green's function is used in the integral of Eq. (1.6). The sound field is then given as a superposition of time-delayed signals emanating from the sources in V. One can regard Eq. (1.6) as the formal solution to the problem if the source term $s(\mathbf{x}, t)$ is independent of the acoustic field and given explicitly. However, if there is a back-reaction of the acoustic field on the source, Eq. (1.6) represents an integral equation for $p'(\mathbf{x}, t)$, rather than an explicit solution for $p'(\mathbf{x}, t)$. Together with the primary source, the back-reaction from the acoustic field forms a feedback loop, and this can lead to self-excited (or self-sustained) oscillations.

The prototype example of a self-excited oscillation in thermoacoustics is the Rijke tube. This is a straight vertical tube with open ends and a hot gauze stretched across its cross-section. Under certain conditions, the tube emits a loud booming sound, with just one (or a few) dominant frequencies, which are close to the tube's resonance frequencies. This is generated by the feedback between the acoustic field (similar to that in an organ pipe) and the fluctuations of the rate of heat released from the hot gauze. The hot gauze acts like a monopole-type sound source [22]. This phenomenon is called "thermoacoustic instability". It also occurs in combustion systems if the acoustic field in the combustion chamber interacts with the flame dynamics. More information on Rijke tubes can be found in [23].

Aeroacoustic instabilities occur in various flow-duct systems and are due to the interaction between unsteady fluctuations in the flow (such as an oscillating shear layer or eddies) and the acoustic modes in a resonating component of the duct system. Human whistling is an example of such an instability. Another example is the sound produced by an aperture in a flow duct. By forcing a flow through the aperture, a jet is created on the downstream side of the aperture; this creates a vorticity distribution, which in turn acts like dipole-type source of sound [24]. This phenomenon tends to manifest itself by a whistling tone and it is called "aeroacoustic instability".

Studies, based on the tailored Green's function, of self-excited oscillations in thermoacoustics and aeroacoustics exist, but are quite rare.

- Heckl and Howe [21] predicted the growth rates of thermoacoustic instabilities in a quasi-1D enclosure with a localised blockage as well as jumps in cross-section and mean temperature.
- Bigongiari and Heckl [25] considered a duct housing a flame which was coupled to the acoustic field by an amplitude-dependent time-lag law and investigated nonlinear effects (limit cycles, bistability, hysteresis).
- Wang and Heckl [26] performed a fundamental study of thermoacoustic instabilities in a hard-walled box.
- Su et al. [27] used a tailored Green's function to predict the acoustic characteristics of an in-duct aperture with bias flow, but did not study self-sustained oscillations.

The configuration we will consider is quite basic, consisting of just two components (see Fig. 1):

(1) a one-dimensional acoustic resonator,

(2) a compact source, which reacts to the acoustic field in the resonator.

The acoustic resonator is a duct of finite length L without mean flow. Section 2 gives the governing equations for its tailored Green's function, as well as explicit analytical expressions in the form of a superposition of duct modes. The acoustic source is described in Section 3. It is located at the axial position x_q in the duct (see Fig. 1); its extent in the axial direction is much smaller than the duct length. We treat it as a narrow control volume across which the acoustic pressure and velocity are discontinuous. The coupling between the resonator and the source will be modelled by integral equations for the acoustic pressure and velocity. These will be derived in Section 4 from the acoustic analogy equation and a feedback model for the acoustic source. Examples to demonstrate the predictive value of this approach will be shown in Section 5. Our model can be extended in several directions, and these will be described in Section 6.

2. Duct model in terms of the tailored Green's function for the acoustic pressure and velocity

We consider the duct shown in Fig. 1. Its ends at $x = 0$ and $x = L$ are assumed to be open and have pressure reflection coefficients

$$R_0 = -1, \quad R_L = -1\,. \tag{2.1a,b}$$

The boundary conditions for the acoustic pressure p' are then given by

$$p'(x,t)\big|_{x=0} = p'(x,t)\big|_{x=L} = 0\,, \tag{2.2a,b}$$

and for the acoustic velocity u' by

$$\left.\frac{\partial u'}{\partial x}\right|_{x=0} = \left.\frac{\partial u'}{\partial x}\right|_{x=L} = 0\,. \tag{2.3a,b}$$

We introduce two separate Green's functions for the pressure and velocity:

G_p, which satisfies the pressure boundary conditions (Eq. (2.2))

G_u, which satisfies the velocity boundary conditions (Eq. (2.3))

Both satisfy the PDE

$$\frac{1}{c^2}\frac{\partial^2 G}{\partial t^2} - \frac{\partial^2 G}{\partial x^2} = \delta\left(x - x^*\right)\,\delta\left(t - t^*\right)\,, \tag{2.4}$$

where x and t are the observer position and observer time, respectively; x^* is the position of a hypothetical impulsive point source, and t^* is the firing time of the impulse. They can be calculated analytically, giving the following results,

$$G_p\left(x, x^*, t - t^*\right) = \begin{cases} H\left(t - t^*\right)\dfrac{2c}{\pi}\displaystyle\sum_{n=1}^{\infty}\frac{(-1)^n}{n}\sin\frac{\omega_n x}{c}\,\sin\frac{\omega_n\left(x^* - L\right)}{c}\,\sin\omega_n\left(t - t^*\right) & \text{for } x < x^* \\ H\left(t - t^*\right)\dfrac{2c}{\pi}\displaystyle\sum_{n=1}^{\infty}\frac{(-1)^n}{n}\sin\frac{\omega_n\left(x - L\right)}{c}\,\sin\frac{\omega_n x^*}{c}\,\sin\omega_n\left(t - t^*\right) & \text{for } x > x^* \end{cases} \tag{2.5}$$

and

$$G_u\left(x, x^*, t - t^*\right) = \begin{cases} H\left(t - t^*\right)\dfrac{2c}{\pi}\displaystyle\sum_{n=1}^{\infty}\frac{(-1)^n}{n}\cos\frac{\omega_n x}{c}\,\cos\frac{\omega_n\left(x^* - L\right)}{c}\,\sin\omega_n\left(t - t^*\right) & \text{for } x < x^* \\ H\left(t - t^*\right)\dfrac{2c}{\pi}\displaystyle\sum_{n=1}^{\infty}\frac{(-1)^n}{n}\cos\frac{\omega_n\left(x - L\right)}{c}\,\cos\frac{\omega_n x^*}{c}\,\sin\omega_n\left(t - t^*\right) & \text{for } x > x^* \end{cases} \tag{2.6}$$

(see Appendix D). In both results

$$\omega_n = \frac{n\pi c}{L} \tag{2.7}$$

denotes the frequency of duct mode n, and $H(t - t^*)$ denotes the Heaviside function. Both Green's functions satisfy causality,

$$G\left(x, x^*, t - t^*\right) = 0 \quad \text{for} \quad t^* \geq t\,, \tag{2.8a}$$

$$\frac{\partial}{\partial t}G\left(x, x^*, t - t^*\right) = 0 \quad \text{for} \quad t^* \geq t\,, \tag{2.8b}$$

and reciprocity,

$$G\left(x, x^*, t - t^*\right) = G\left(x^*, x, t - t^*\right)\,. \tag{2.9}$$

3. Model for the source

The source produces a discontinuity of the acoustic field across the control volume. We utilise this feature to describe the source in terms of jump conditions for the acoustic pressure and velocity. Two different perspectives will be adopted. The first (presented in Section 3.1) focusses on physical insight, while the second (presented in Section 3.2) takes advantage of the transfer matrix method, which is popular for the analysis of one-dimensional acoustic systems.

3.1. Jump conditions due to fluctuating heat source and external force

We derive the jump conditions from the conservation equations for mass and momentum.

3.1.1. Jump condition for the acoustic velocity

The linearised mass conservation equation is

$$\frac{\partial \rho'}{\partial t} + \bar{\rho}\frac{\partial u'}{\partial x} = 0\,, \tag{3.1}$$

(see [28], section 4.2), where ρ is the density; the overbar denotes the mean part, and the prime $'$ denotes the perturbation part. We add the term $\frac{1}{c^2}\frac{\partial p'}{\partial t}$ to both sides of Eq. (3.1) and obtain

$$\frac{1}{c^2}\frac{\partial p'}{\partial t} + \bar{\rho}\frac{\partial u'}{\partial x} = \frac{\partial}{\partial t}\left(\frac{p'}{c^2} - \rho'\right)\,. \tag{3.2}$$

The right-hand side can be expressed in terms of the rate of heat release (see [29], section 7.3),

$$\frac{\partial}{\partial t}\left(\frac{p'}{c^2} - \rho'\right) = \frac{\gamma - 1}{c^2}\,\bar{\rho}\,q'(x,t)\,, \tag{3.3}$$

where $q'(x,t)$ is the distribution of the heat release rate per unit mass (it has units W kg^{-1}). The equation for mass conservation then becomes

$$\frac{1}{c^2}\frac{\partial p'}{\partial t} + \bar{\rho}\frac{\partial u'}{\partial x} = B\,q'(x,t)\,, \tag{3.4}$$

where the constant B has been introduced as abbreviation for

$$B = \frac{\gamma - 1}{c^2}\bar{\rho}\,. \tag{3.5}$$

Given that heat release only occurs inside the control volume, we can express it by

$$q'(x,t) = Q'(t)\,\delta(x - x_q)\,, \tag{3.6}$$

where x_q is the position of the control volume, and $Q'(t)$ is a measure for the time-dependence of the overall heat release rate. We can then write Eq. (3.4) as

$$\frac{1}{c^2}\frac{\partial p'}{\partial t} + \bar{\rho}\frac{\partial u'}{\partial x} = B\,Q'(t)\,\delta(x - x_q)\,, \tag{3.7}$$

We now integrate Eq. (3.7) over the narrow range between $x_q - \Delta x$ and $x_q + \Delta x$ along the x-axis, and then let $\Delta x \to 0$. This gives

$$u_2' - u_1' = \frac{B}{\bar{\rho}}Q'(t)\,, \tag{3.8}$$

which relates the velocity jump $u_2' - u_1'$ to the heat release rate in the control volume. It is in line with the well-known fact that an unsteady heat release rate acts like an acoustic monopole.

3.1.2. Jump condition for the acoustic pressure

We start the derivation with the linearised momentum equation (see [28], section 4.2)

$$\bar{\rho}\frac{\partial u'}{\partial t} + \frac{\partial p'}{\partial x} = f'(x,t)\,, \tag{3.9}$$

where $f'(x,t)$ represents an external force distribution, which could come, for example, from the inertia of a plug of fluid in an orifice (it has units N m^{-3}). Since this force distribution is non-zero only in the control volume, it can be expressed as

$$f'(x,t) = F'(t)\,\delta(x - x_q) \tag{3.10}$$

(in analogy to Eq. (3.6)), where $F'(t)$ is a measure for the time-dependence of the overall force. Again, we integrate Eq. (3.9) over the narrow range between $x_q - \Delta x$ and $x_q + \Delta x$, and then let $\Delta x \to 0$. This leads to

$$p_2' - p_1' = F'(t)\,, \tag{3.11}$$

which relates the pressure jump $p_2' - p_1'$ to the force in the control volume. It is in line with the well-known fact that an unsteady force acts like an acoustic dipole.

3.2. Jump conditions in terms of the transfer matrix

An alternative way to describe the jump conditions is to regard the control volume as an input/output system, where the upstream edge forms the input side, and the downstream edge forms the output side. Then the control volume can be represented in the frequency-domain by a transfer matrix $\mathbf{T}$ [30]. This is a 2×2 matrix, which relates the acoustic field quantities on the downstream edge (subscript 2) to those on the upstream edge (subscript 1),

$$\begin{bmatrix} \hat{p}_2 \\ \hat{u}_2 \end{bmatrix} = \begin{bmatrix} T_{11} & T_{12} \\ T_{21} & T_{22} \end{bmatrix} \begin{bmatrix} \hat{p}_1 \\ \hat{u}_1 \end{bmatrix}\,; \tag{3.12}$$

the hat ˆ denotes frequency-domain quantities. The matrix elements T_{11}, T_{12}, T_{21} and T_{22} are generally complex and frequency-dependent, and they can be measured for a given configuration (see e.g. [31,32]).

The elements of the transfer matrix are linked to the source terms in the frequency domain, $\hat{F}(\omega)$ and $\hat{Q}(\omega)$, which are the Fourier transforms of $F'(t)$ and $Q'(t)$, respectively. This can be seen by rewriting Eq. (3.12) as two separate equations for the pressure jump and velocity jump,

$$\hat{p}_2 - \hat{p}_1 = (T_{11} - 1)\,\hat{p}_1 + T_{12}\,\hat{u}_1\,, \tag{3.13}$$

$$\hat{u}_2 - \hat{u}_1 = T_{21}\,\hat{p}_1 + (T_{22} - 1)\,\hat{u}_1\,. \tag{3.14}$$

Comparison with the jump conditions, Eqs. (3.8) and (3.11), shows that

$$\hat{F}(\omega) = (T_{11} - 1)\,\hat{p}_1 + T_{12}\,\hat{u}_1\,, \tag{3.15}$$

$$\hat{Q}(\omega) = \frac{\bar{\rho}}{B}\left[T_{21}\,\hat{p}_1 + (T_{22} - 1)\,\hat{u}_1\right]\,. \tag{3.16}$$

These two equations can in principle be transformed into the time-domain to give $F'(t)$ and $Q'(t)$ in terms of p'_1 and u'_1 at the current time t and earlier times.

4. Integral governing equations for the time histories of pressure and velocity

We will derive two integral equations; one is based on the analogy equation for the pressure; this is shown in Section 4.1. The subsequent Section 4.2 shows the derivation for the velocity.

4.1. Governing equation for the pressure

The acoustic analogy equation can be derived by simple manipulations of the conservation equations for mass and momentum, given by Eqs. (3.4) and (3.9), respectively. We differentiate Eq. (3.4) with respect to t, Eq. (3.9) with respect to x, and then subtract the resulting equations. In this way, the velocity u' gets eliminated from the equations, and we obtain

$$\frac{1}{c^2}\frac{\partial^2 p'}{\partial t^2} - \frac{\partial^2 p'}{\partial x^2} = B\,\frac{\partial q'}{\partial t} - \frac{\partial f'}{\partial x}\,. \tag{4.1}$$

This is the acoustic analogy equation for the pressure. The left hand side of Eq. (4.1) has the same form as that of Eq. (2.4), which defines the Green's function. We exploit this feature to combine the two Eqs. (2.4) and (4.1), and derive an integral equation for the pressure. This requires a series of mathematical manipulations (in particular using integration by parts, applying the boundary conditions in Eq. (2.2) and making use of the causality conditions in Eq. (2.8) and reciprocity in Eq. (2.9)), which are shown in Appendix A. The result is

$$p'(x,t) = -B\int_{t^*=0}^{t} \left.\frac{\partial G_p}{\partial t^*}\right|_{x^*=x_q} Q'(t^*)\,\mathrm{d}t^* + \int_{t^*=0}^{t} \left.\frac{\partial G_p}{\partial x^*}\right|_{x^*=x_q} F'(t^*)\,\mathrm{d}t^* \quad + \quad \text{i.c.}\,. \tag{4.2}$$

This is the governing equation for the acoustic pressure. The abbreviation i.c. denotes a term, which depends on the initial conditions for p' at $t = 0$. The integrals in Eq. (4.2) have the source time t^* as integration variable. Hence Eq. (4.2) gives the pressure $p'(x,t)$ at the observer time t in terms of the heat release rate $Q'(t^*)$ and the force $F'(t^*)$ at earlier times.

4.2. Governing equation for the velocity

Again, we first construct an analogy equation as basis for the integral governing equation for the velocity. In order to eliminate the pressure (rather than the velocity) from the conservation equations, we divide the mass equation (Eq. (3.4)) by $\bar{\rho}$ and differentiate it with respect to x, while we divide the momentum equation (Eq. (3.9)) by $\bar{\rho}c^2$ and differentiate it with respect to t. Subtraction of the resulting equations leads to

$$\frac{1}{c^2}\frac{\partial^2 u'}{\partial t^2} - \frac{\partial^2 u'}{\partial x^2} = -\frac{B}{\bar{\rho}}\frac{\partial q'}{\partial x} + \frac{1}{\bar{\rho}\,c^2}\frac{\partial f'}{\partial t}\,. \tag{4.3}$$

This is the acoustic analogy equation for the velocity. The left hand side of this equation has again the same form as that of Eq. (2.4), which defines the Green's function. By combining Eq. (2.4) for G_u and Eq. (4.3) (see Appendix A), we obtain the integral equation

$$u'(x,t) = \frac{B}{\bar{\rho}}\int_{t^*=0}^{t} \left.\frac{\partial G_u}{\partial x^*}\right|_{x^*=x_q} Q'(t^*)\,\mathrm{d}t^* - \frac{1}{\bar{\rho}c^2}\int_{t^*=0}^{t} \left.\frac{\partial G_u}{\partial t^*}\right|_{x^*=x_q} F'(t^*)\,\mathrm{d}t^* \quad + \quad \text{i.c.}\,. \tag{4.4}$$

Table 1
Parameters describing the nonlinear Rijke tube.

Parameter	Symbol	Numerical value	Units
Tube length	L	1	m
Mean temperature of the air	$\bar{T}$	623	K
Speed of sound	c	495	m s^{-1}
Velocity of the mean flow	$\bar{u}$	1.0	m s^{-1}
Time-lag	τ	0.0036	s
Measure for flame power	b	2.09×10^5	W m kg^{-1}
Coupling coefficient for linear part	n_0	1	
Coupling coefficient for nonlinear part	n_1	−17.4	
Heat source position	x_q	0.1, 0.3, 0.7, 0.9	m

4.3. Numerical solution of the integral governing equations

We evaluate the governing equations, Eqs. (4.2) and (4.4), at $x = x_q^+$, i.e. at the upstream edge of the control volume,

$$p_1'(t) = -B \int_{t^*=0}^{t} \left.\frac{\partial G_p}{\partial t^*}\right|_{\substack{x=x_q \\ x^*=x_q}} Q'(t^*)\,\mathrm{d}t^* + \int_{t^*=0}^{t} \left.\frac{\partial G_p}{\partial x^*}\right|_{\substack{x=x_q \\ x^*=x_q}} F'(t^*)\,\mathrm{d}t^* \quad + \quad \text{i.c.}\,, \tag{4.5}$$

$$u_1'(t) = \frac{B}{\bar{\rho}} \int_{t^*=0}^{t} \left.\frac{\partial G_u}{\partial x^*}\right|_{\substack{x=x_q \\ x^*=x_q}} Q'(t^*)\,\mathrm{d}t^* - \frac{1}{\bar{\rho}c^2} \int_{t^*=0}^{t} \left.\frac{\partial G_u}{\partial t^*}\right|_{\substack{x=x_q \\ x^*=x_q}} F'(t^*)\,\mathrm{d}t^* \quad + \quad \text{i.c.} \tag{4.6}$$

The derivatives of the Green's functions G_p and G_u in the integrands can be evaluated from Eqs. (2.5) and (2.6), and are known. The source terms $Q'(t^*)$ and $F'(t^*)$ ($t^* = 0, \ldots, t$) depend on the acoustic field p_1' and u_1'. The two Eqs. (4.5) and (4.6) therefore represent a set of two coupled integral equations of the Volterra type [33] for the unknown functions $p_1'(t)$ and $u_1'(t)$. These functions occur at the current time t on the left hand side, and at earlier times in the integrals on the right hand side. It is straightforward to solve these integral equations numerically with an iterative approach stepping forward in time. This is described in Appendix B. The numerical effort is kept low by exploiting the fact that the Green's function is known analytically, which makes it possible to sidestep the need to sum over an ever-increasing number of terms as the iteration proceeds.

If the dependence of the source terms is given in the frequency domain as functions of $\hat{p}_1(\omega)$ and $\hat{u}_1(\omega)$ (as, for example, in Eqs. (3.15) and (3.16)), these will have to be converted into the time-domain. This is described in Appendix C.

5. Some examples

In this section, we show three examples, where we apply the framework based on the tailored Green's function. The first example is a Rijke tube with a strongly nonlinear heat release law (Section 5.1). The second example is a flow duct with an orifice, which has the potential to whistle (Section 5.2). In the third example (Section 5.3), we consider a duct with *two* acoustic sources: an orifice plate (dipole source) anchoring a flame (monopole source).

In all examples, the resonator is a duct with open ends, zero radiation losses and no friction. It is described by the Green's functions given by Eqs. (2.5) and (2.6). The first two modes are included; higher modes are ignored. The results are calculated by solving Eqs. (4.5) and (4.6) with the iteration scheme described in Appendices B and C. The time step in the iteration is $\Delta t = 10^{-5}$ s throughout.

In real systems, instabilities arise spontaneously, rather than at some initial time. We assume that we have a perfect active control system, proposed by Ffowcs Williams, which for $t < 0$ suppresses any instability generated by the heat source or by the flow through the orifice. At $t = 0$, the active control system is switched off instantly. The system is then free to become unstable, i.e. the oscillation amplitude can grow, starting from a small initial value, triggered, for example, by low-level broadband noise.

5.1. The nonlinear Rijke tube

In this section, we consider a Rijke tube with a strongly nonlinear heat release rate law. The air in the tube has uniform properties: the mean temperature is $\bar{T} = 623$ K, and the corresponding speed of sound is $c = 495$ m s^{-1}. The tube is 1 m long; its first two modes have frequencies $f_1 = 248$ Hz, $f_2 = 496$ Hz, and periods $T_1 = 0.0040$ s, $T_2 = 0.0020$ s. We assume that the heat release rate is described by the Levine–Baum formulation [34]

$$Q'(t) = -b \left[n_1 \frac{|u_1'(t-\tau)|}{\bar{u}} + n_0 \right] \frac{u_1'(t-\tau)}{\bar{u}}\,. \tag{5.1}$$

The symbols are explained in Table 1 (columns 1 and 2, rows 5–8).

The numerical iteration scheme described in Appendix B is used, with $F'(t) = 0$ throughout, to calculate the time histories. In Figs. 2 and 3, we present results for the parameter values listed in Table 1. The heat source position was varied, taking values x_q =0.1, 0.3, 0.7, 0.9 m. The initial conditions were $Q'(t)|_{t=0} = 10^{-6}$ W m kg^{-1}, $u_1'(t)|_{t=0} = 10^{-6}$ m s^{-1}. Fig. 2 shows the results for

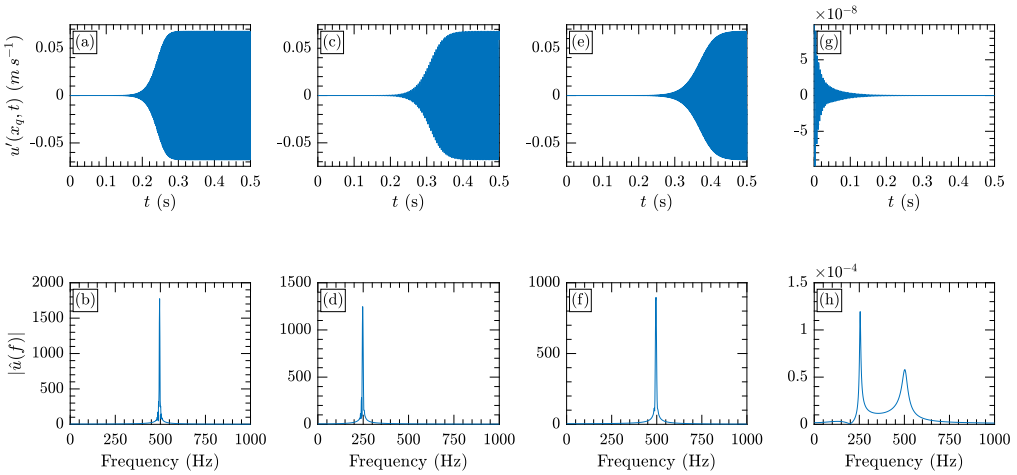

Fig. 2. Velocity results for four heat source positions x_q. Top row: time histories; bottom row: frequency spectra. (a,b): x_q = 0.1 m ; (c,d): x_q = 0.3 m ; (e,f) x_q = 0.7 m ; (g,h) x_q = 0.9 m.

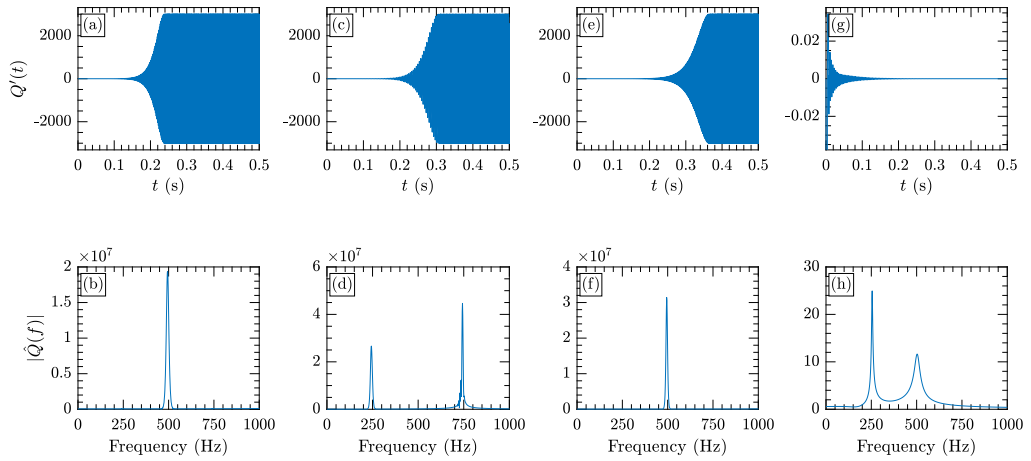

Fig. 3. Results for the heat release rate for four heat source positions x_q. Top row: time histories; bottom row: frequency spectra. (a,b): x_q = 0.1 m ; (c,d): x_q = 0.3 m ; (e,f) x_q = 0.7 m ; (g,h) x_q = 0.9 m.

the acoustic velocity at the heat source, and Fig. 3 shows the results for the heat release rate. The top row of these figures shows the time histories, and the bottom row shows the corresponding frequency spectra. The time histories display the envelopes of the oscillations; the oscillations themselves are not visible, but their frequency content can be seen in the spectra.

The heat release rate law in Eq. (5.1) has a linear term, $n_0 \frac{u_1'(t-\tau)}{\bar{u}}$, and a nonlinear term, $n_1 \frac{|u_1'(t-\tau)|u_1'(t-\tau)}{\bar{u}^2}$. With the coupling coefficients given by the values in Table 1, the linear term dominates for small velocity amplitudes of up to about 0.05 m s^{-1}, while the nonlinear term dominates for higher amplitudes. The "competition" between the two terms manifests itself in the velocity time histories shown in Figs. 2(a), (c) and (e): the exponential growth at low amplitudes is followed by a limit cycle with an amplitude of about 0.07 m s^{-1}. The corresponding spectra underneath reveal which mode appears in the limit cycle. For x_q = 0.1 m, both modes are linearly unstable, but only mode 2 appears in the limit cycle. For x_q = 0.3 m, only mode 1 is linearly unstable, and this mode appears in the limit cycle. Mode 2 behaves in the same way for x_q = 0.7 m. For x_q = 0.9 m, both modes are linearly stable, the oscillation decays, and there is no limit cycle.

Looking at the spectra in Fig. 3 for the heat release rate, we observe additional peaks at higher frequencies, which are not present in the velocity spectra. These peaks are harmonics due to the nonlinear nature of the heat release rate law in Eq. (5.1). The effect on the acoustic field of any harmonics above about 500 Hz is not captured here because our Green's function includes only the first two modes (mode 2 has frequency f_2 = 496 Hz). If higher frequencies in the acoustic field are of interest, more modes need to be included in the Green's function.

The Galerkin method [35], [36, section 4.3] would offer an alternative to our Green's function approach in that it would give time histories resembling the ones presented here for nonlinear heat release laws. Like our Green's function approach, the Galerkin

Table 2
Parameters describing the duct and the orifice.

Parameter	Symbol	Numerical value	Units
Duct length	L	0.8	m
Speed of sound	c	348	m s^{-1}
Position of orifice plate	x_q	0.28	m
Thickness of orifice plate	t_o	0.003	m
Orifice diameter	D_o	0.01	m
Bias flow velocity	$\bar{u_o}$	2.52	m s^{-1}
Reynolds number of bias flow	Re	1600	

method is based on the analogy equation Eq. (4.1) with localised sources described in terms of delta functions as in Eqs. (3.6) and (3.10). In the Galerkin method, a trial solution of the form

$$p'(x,t) = \sum_{n=1}^{N} \eta_n(t)\,\psi_n(x) \tag{5.2}$$

is used, which represents a superposition of duct modes. $\eta_n(t)$ is the (unknown) time-dependence of mode n, and $\psi_n(x)$ is the corresponding (known) eigenfunction. Second-order ODEs for $\eta_n(t)$ can be derived by the following mathematical steps:

- substitute Eq. (5.2), together with Eqs. (3.6) and (3.10), into Eq. (4.1);
- multiply the resulting equation by $\psi_m(x)$ and integrate it over the tube length;
- exploit the orthogonality of the functions $\psi_n(x)$ to get individual ODEs for $\eta_n(t)$.

The resulting ODEs are coupled forced oscillator equations, i.e.

$$\frac{\mathrm{d}^2\eta_n}{\mathrm{d}t^2} + \omega_n^2\eta_n = \text{forcing term}\,, \tag{5.3}$$

where the forcing term depends (linearly or nonlinearly) on the acoustic field at the source position, which includes not just mode n, but also the other modes. The set of ODEs needs to be solved numerically, for example by a Runge–Kutta scheme. The advantage of our Green's function approach over the Galerkin method is that we are dealing with an integral formulation and therefore random errors in the numerical process are smoothed out [6].

5.2. The whistling orifice

In this section, we consider an orifice in a finite-length flow duct. Such a set-up is known to whistle under certain circumstances [37].

Our duct has ideal open ends with zero radiation losses. Losses due to friction are not included either. The temperature in the duct is uniform and associated with a speed of sound $c = 348$ m s^{-1}. The duct is 0.8 m long; its first two modes have frequencies $f_1 = 218$ Hz and $f_2 = 436$ Hz. The orifice plate is located in the duct at the axial position $x_q = 0.35L = 0.28$ m; its thickness is $t_o = 0.003$ m. The orifice diameter is $D_o = 0.01$ m, giving an aspect ratio of $t_o/D_o = 0.3$. The mean flow in the duct creates a bias flow with velocity $\bar{u}_o$ in the orifice; the corresponding Reynolds number is $Re = D_o\bar{u}_o/\nu$, where ν is the kinematic viscosity. The duct diameter and the mean flow velocity in the duct have no influence on the results.

The parameters describing the duct and the orifice are summarised in Table 2.

We assume that the hydrodynamic effects in and around the orifice can be modelled by a dipole force given in terms of a transfer impedance $Z(\omega)$,

$$\hat{F}(\omega) = Z(\omega)\,\hat{u}_1(\omega)\,. \tag{5.4}$$

Several results for $Z(\omega)$ are available in the literature. We choose the transfer impedance, which has been determined by Fabre et al. [38] by numerically solving the incompressible linearised Navier–Stokes equations for the flow through a circular orifice in a thick plate. Their transfer impedance is shown in Fig. 4 as a function of frequency for an orifice with the properties given in Table 2. Fig. 4(a) shows the real part (resistance), and Fig. 4(b) shows the imaginary part (reactance). We have converted their results, which are given in terms of the Strouhal number ($St = \omega D_o/(2\bar{u}_o)$), to results along the frequency axis and adapted them to our notation.

In our notation, the sign of the resistance, $\mathrm{Re}\,(Z(\omega))$ is such that it describes damping if $\mathrm{Re}\,(Z(\omega)) < 0$ and amplification if $\mathrm{Re}\,(Z(\omega)) > 0$. The resistance in Fig. 4(a) is positive in the frequency ranges $[153 \cdots 287]$ Hz and $[603 \cdots 740]$ Hz. The lower frequency range corresponds to the first hydrodynamic mode, and the higher one corresponds to the second harmonic mode [39]. This indicates that the orifice might act as an amplifier if it is situated inside a duct, i.e. coupled to an acoustic resonator.

Here, the source is not described in the time-domain, but in the frequency-domain as shown in Fig. 4. In order to solve the integral equations, Eqs. (4.5) and (4.6), it is necessary to transform $\hat{F}(\omega)$ into $F'(t)$. We do this with a two-step procedure: In the first step (using MATLAB's `rationalfit` routine), we represent $Z(\omega)$ by a series of rational functions, each with two fitting parameters; these are determined numerically by least-squares fitting, minimising the discrepancy with the curves in Fig. 4. In the second step, we transform the rational function representation into the time-domain (see Appendix C, where the procedure is described in more detail).

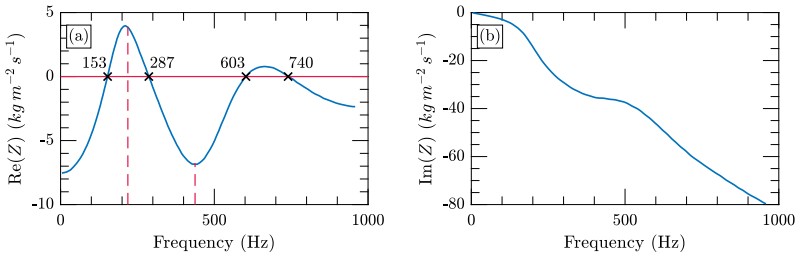

Fig. 4. Transfer impedance for an orifice with the properties given in Table 2 (adapted from Fig. 7(e) in [38]); (a) real part (resistance), (b) imaginary part (reactance). The dashed vertical lines mark the frequencies of the first two eigenmodes of our duct.

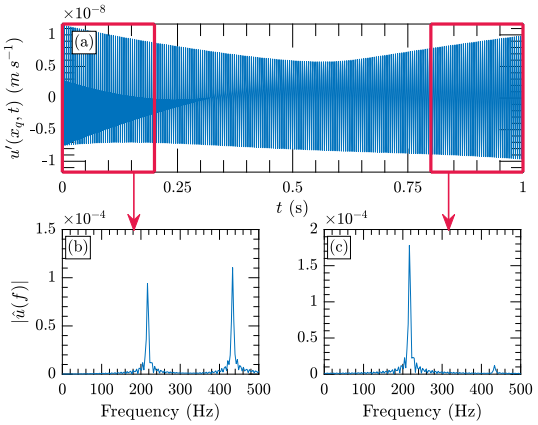

Fig. 5. Results for the acoustic velocity; (a) time history; (b) frequency spectra for the time interval [0 … 0.2]s (left); (c) frequency spectrum for the time interval [0.8 … 1.0]s (right).

Fig. 5 shows our predictions for the acoustic velocity (measured on the upstream side of the orifice plate); Fig. 5(a) gives the time history; the two red boxes mark two time windows: one at the beginning and one at the end of the time history. Fig. 5(b) gives the frequency spectrum for the early time window, and Fig. 5(c) gives that for the late time window.

The Green's function included modes 1 and 2, but no higher modes. The oscillation was triggered by imposing the initial force $F'(t)|_{t=0} = 10^{-3}$ N m^{-2}, while $Q'(t)|_{t=0} = 0$.

The time history of the acoustic velocity, which is shown in Fig. 5(a), looks rather peculiar because it includes mode 1 and mode 2. The stability behaviour of the individual modes can be discerned from the frequency spectra shown in Figs. 5(b) and (c). Mode 1 (218 Hz) clearly increases in amplitude. Further spectra (not shown) calculated for time windows between the two red ones marked in Fig. 5(a) confirm that the increase of mode 1 is exponential. Mode 2 (436 Hz) is stable. It starts with an amplitude higher than that of mode 1, but decays exponentially and is barely detectable at the end of the time history.

The corresponding results for the dipole force are shown in Fig. 6. It is evident that the dipole force features the same qualitative behaviour as the acoustic velocity. This behaviour is expected, given that the frequency of mode 1 is in the range where the resistance is positive, while mode 2 has a frequency where the resistance is negative (see Fig. 4).

We have validated our results obtained from the Green's function approach by calculating the complex eigenfrequencies of modes 1 and 2 with an eigenvalue approach. The predictions of both approaches were fully consistent.

5.3. Duct with a flame anchored on an orifice plate

We consider the configuration shown in Fig. 7, consisting of a uniform duct of length L; both ends of the duct are open.

An orifice plate is positioned in the duct at the axial position x_q. A premixed gas passes through the orifice and is burnt in a flame that is anchored on the downstream edge of the hole. We treat the orifice plate and the flame as two individual acoustic sources at the same axial position; both sources are linear. The parameters for this set-up are listed in Table 3.

We describe the orifice plate by the same transfer impedance as in Section 5.2 (see Figs. 4(a) and (b)). Whether the orifice plate acts as an amplifier or a damper of a particular mode depends on the frequency of that mode, which in turn depends on the length of the duct.

The flame is modelled as a monopole source, which we describe here by a simple time-lag law for the heat release rate,

$$Q'(t) = n\,u'_1(t-\tau)\,, \tag{5.5}$$

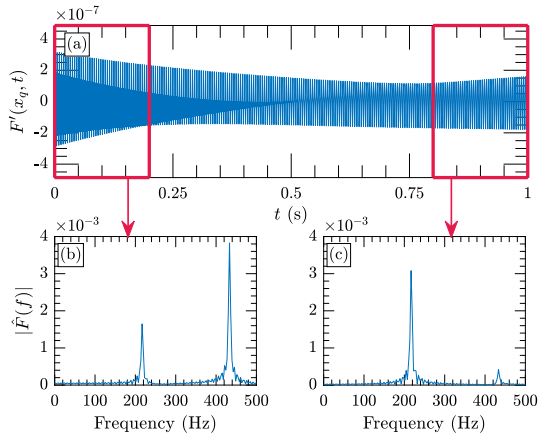

Fig. 6. Results for the dipole force; (a) time history; (b) frequency spectra for the time interval [0 … 0.2]s (left); (c) frequency spectrum for the time interval [0.8 … 1.0]s (right).

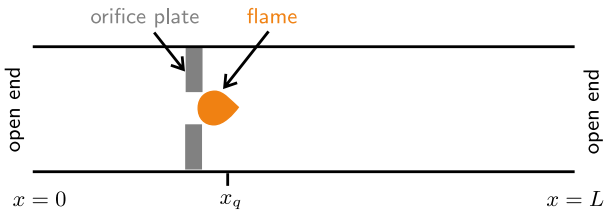

Fig. 7. Duct with orifice plate, flame and open ends.

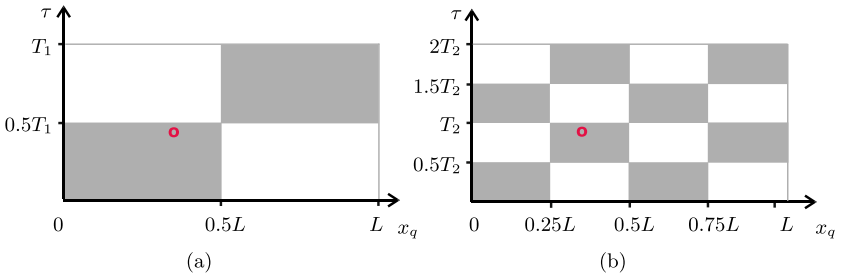

Fig. 8. Map of the Rayleigh index in the $x_q\tau$ – plane for the first two modes of the duct, (a) mode 1 and (b) mode 2. Grey regions denote positive, white regions denote negative Rayleigh index. The small red circle marks the parameter values $x_q = 0.35L$, $\tau = 0.45T_1 = 0.89T_2$.

where n is the coupling coefficient and τ is the time-lag. According to the Rayleigh criterion, τ and x_q are the critical parameters that determine whether the flame acts as an amplifier or damper for a particular mode. Fig. 8 shows the sign of the Rayleigh index $\overline{p'(t)Q'(t)}$ (the overbar denotes the time-average) in the $x_q\,\tau$ – plane for the first two modes of an open-ended duct. Grey regions denote positive Rayleigh index (amplifier), while white regions denote negative Rayleigh index (damper). The point $x_q = 0.35L$, $\tau = 0.45T_1 = 0.89T_2$, which we consider here, lies in regions of positive Rayleigh index (marked by a small red circle), so the flame acts as an amplifier for both modes.

We perform two parameter studies in the two subsections below to illustrate some effects that can occur when the orifice plate and the flame are put together. The properties of the complete system are listed in Table 3. In Section 5.3.1, we vary the *flame power* by increasing the coupling coefficient n. The initial conditions were $F'(t)|_{t=0} = 10^{-6}$ N m^{-2}, $Q'(t)|_{t=0} = 10^{-6}$ W m kg^{-1}, $p_1'(t)|_{t=0} = 10^{-3}$ N m^{-2} and $u_1'(t)|_{t=0} = 10^{-3}$ m s^{-1}. Their choice was motivated by the aim to obtain results that could be displayed well and interpreted clearly.

In Section 5.3.2, we vary the frequencies of the two modes by varying the *duct length*. In both subsections, we show the time histories $p_1'(t)$ and $u_1'(t)$, as well as the corresponding frequency spectra.

Table 3
Parameters describing the setup shown in Fig. 7.

	Symbol	Numerical value	Units
Duct parameters			
Speed of sound	c	348	m s^{-1}
Length	L	3.0, 1.5, 0.8	m
Frequency of mode 1	f_1	58, 116, 217	Hz
Frequency of mode 2	f_2	116, 232, 434	Hz
Period of mode 1	T_1	17.2, 8.62, 4.61	10^{-3} s
Period of mode 2	T_2	8.62, 4.32, 2.30	10^{-3} s
Orifice plate parameters			
Frequency ranges where $\mathrm{Re}(Z) > 0$		[153 ...287], [603 ...740]	Hz
Axial position	x_q	$0.35L$	m
Flame parameters			
Axial position	x_q	$0.35L$	m
Time-lag	τ	$\tau = 0.45T_1 = 0.89T_2$	s
Coupling coefficient	n	1000, 5000, 10000	W s kg^{-1}

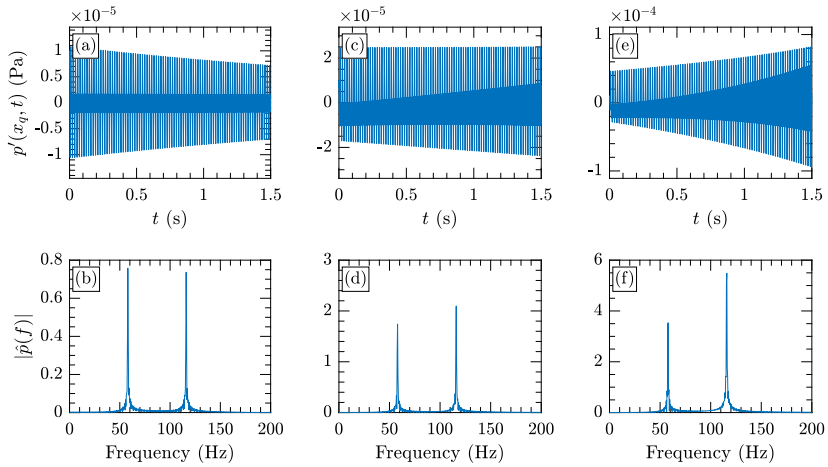

Fig. 9. Pressure results for three coupling coefficients n, with L = 3 m . Top row: time histories; bottom row: frequency spectra. (a,b): n = 1000 W s kg^{-1}; (c,d): n = 5000 W s kg^{-1}; (e,f): n = 10,000 W s kg^{-1}.

5.3.1. Variable flame power

We simulate flames of different powers by varying the coupling coefficient (n = 1000, 5000, 10,000$W\ s\ \mathrm{kg}^{-1}$). The length of the duct is kept constant at L = 3 m. The eigenfrequencies of the first two modes are then f_1 = 58 Hz and f_2 = 116 Hz. They are both in the range where the transfer impedance has a negative real part, i.e. the orifice plate acts as a damper for both modes.

The results for the acoustic pressure are given in Fig. 9, and those for the velocity in Fig. 10; the top rows of these figures show the time histories, and the bottom rows show the corresponding frequency spectra.

From Fig. 9, we make the following observations about the time history and frequency spectrum for the pressure, as the coupling coefficient n increases. For the weakest flame (n = 1000 W s kg^{-1}), the pressure decays with time, indicating that both modes are stable. In this case, the amplifying effect of the flame is not strong enough to overcome the damping effect of the orifice plate. For the strongest flame (n = 10,000 W s kg^{-1}), both modes increase in amplitude, and we conclude that the flame has the upper hand on both modes. For the intermediate flame (n = 5000 W s kg^{-1}), we observe a mixed scenario: mode 1 is damped, but mode 2 is amplified. In all three cases, the spectra show two peaks at 58 Hz and 116 Hz, which are the eigenfrequencies of the duct.

The corresponding results for the velocity are shown in Fig. 10. There are no qualitative differences between the time histories of velocity and pressure. The same is true for the frequency spectra.

5.3.2. Variable duct length

Now we vary the duct length to generate modal frequencies that are inside or outside the frequency ranges, where the orifice plate acts as an amplifier. We consider the two lengths L = 0.8 m and L = 1.5 m. For L = 0.8 m, we have f_1 = 217 Hz ($\mathrm{Re}(Z) > 0$, amplified) and f_2 = 434 Hz ($\mathrm{Re}(Z) < 0$, damped), while for L = 1.5 m the effect on the two modes is the other way round: f_1 = 116 Hz ($\mathrm{Re}(Z) < 0$, damped) and f_2 = 232 Hz ($\mathrm{Re}(Z) > 0$, amplified). The power of the flame is kept constant and low, with the coupling coefficient n = 1000 W s kg^{-1}.

The results for the acoustic pressure are given in Fig. 11, and those for the velocity in Fig. 12; the top rows of these figures show the time histories, and the bottom rows show the frequency spectra.

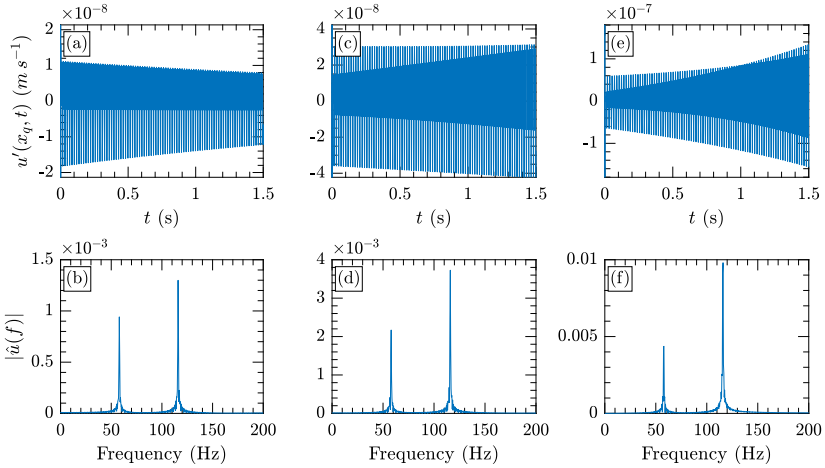

Fig. 10. Velocity results for three coupling coefficients n, with L = 3 m . Top row: time histories; bottom row: frequency spectra. (a,b): n = 1000 W s kg^{-1}; (c,d): n = 5000 W s kg^{-1}; (e,f): n = 10,000 W s kg^{-1}.

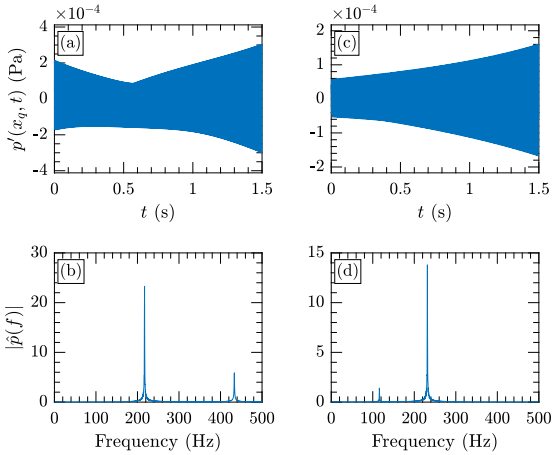

Fig. 11. Pressure results for two duct lengths L, with n = 1000 W s kg^{-1}. Top row: time histories; bottom row: frequency spectra. (a,b): L = 0.8 m ; (c,d): L = 1.5 m.

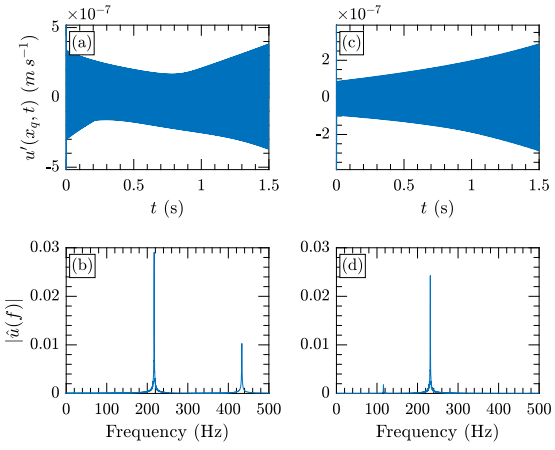

Fig. 12. Velocity results for two duct lengths L, with n = 1000 W s kg^{-1}. Top row: time histories; bottom row: frequency spectra. (a,b): L = 0.8 m ; (c,d): L = 1.5 m.

From Fig. 11 we make the following observations about the time history and frequency spectrum for the pressure. The time history for $L = 0.8$ m has a peculiar envelope. This is due to the fact that we have a superposition of two modes: mode 1 starts with a small amplitude and grows exponentially, while mode 2 starts with a much larger amplitude, but decays. The time history for $L = 1.5$ m shows again a superposition of two modes: here mode 2 grows exponentially and dominates over the damped mode 1 throughout the whole time history.

The corresponding results for the velocity are shown in Fig. 12. There are no qualitative differences between the time histories of velocity and pressure. The same is true for the frequency spectra.

6. Conclusions

Sound generation by a feedback process in an acoustic resonator (e.g. between sound and a flame, or between sound and hydrodynamic structures) is an important topic in several branches of acoustics. For example, feedback between sound and hydrodynamic structures is the underlying mechanism that produces the sound of musical wind instruments. Another example is a thermoacoustic instability, which is due to the feedback between sound and a flame. Multiple feedback, involving sound, flames and hydrodynamic structures, is also possible and has been observed in gas turbine engines amongst other systems.

Our paper introduces a unified framework to study such effects largely analytically, with very little numerical effort. The complete resonator-source system is modelled by a Green's function approach, using the same formalism for aeroacoustic sources and thermoacoustic sources; their coupling to the acoustic field can be linear or nonlinear. Our predictions give time histories for the acoustic field; these are obtained by solving a coupled set of Volterra integral equations with an uncomplicated iteration method, stepping forward in time.

Our method is attractive for fundamental studies and offers several advantages, which have been illustrated by three different case studies:

(1) A Rijke tube with a quadratic dependence of the heat release rate on the acoustic velocity. This case relies on a time-domain approach. The resulting time histories give a wealth of physical information, such as transient behaviour, limit-cycle amplitudes and higher harmonics. Similar results would be obtained from a Galerkin approach; however, our method is less prone to numerical errors since it involves solving integral equations, rather than differential equations. It would be impossible to apply a frequency-domain approach to this case without losing information about the harmonics. Nonlinear approaches in the frequency domain are limited to quasi-nonlinear heat release rate models, where the nonlinearity is merely an amplitude dependence; a common example would be a network model where the flame is described by an amplitude-dependent flame transfer function.

(2) An orifice in a thick plate with bias flow, described by a transfer impedance. We illustrated with this case that our approach can also be used for sources that are described in the frequency domain.

(3) An acoustic resonator with both thermoacoustic feedback (flame) and aeroacoustic feedback (orifice plate). Since little numerical effort is required to produce time histories of the acoustic field and the source terms, parameter studies can be performed quickly, and they give insight into the role of the individual feedback mechanisms, as well as their interaction with each other.

Various extensions of our Green's function approach are feasible: More elaborate resonator geometries can be considered, as long as the tailored Green's function can be calculated analytically. This is the case for a surprisingly diverse group of configurations, for example for ducts with general end conditions, as well as for segmented ducts, where segments with different properties are joined together; these segments could, for example, have different mean temperatures and/or different cross-sectional areas. Furthermore, several sources, at different positions in the resonator cavity, could be added, as long as they can be regarded as acoustically compact. This includes "responsive sources", which react to the acoustic field in the resonator (like the ones showcased in this paper), as well as unresponsive ones (such as external noise). Non-compact sources could also be simulated by a series of closely-spaced compact sources.

Data availability

Data will be made available on request.

Acknowledgements

Aswathy Surendran is a EuroTech Postdoc fellow at the Technische Universität München. The EuroTech Postdoc Programme is co-funded by the European Commission under its framework programme Horizon 2020. Grant Agreement number 754462. We are grateful to Professor Mico Hirschberg for his many constructive suggestions on the manuscript.

Appendix A. Derivation of the integral equations for the pressure and velocity

We derive the integral equation for the *pressure* from the governing PDEs for G_p (see Eq. (2.4)) and p' (see Eq. (4.1)). In a first step, we apply the Laplace transform to both sides of the PDEs, using the following notation and properties:

$$\mathcal{L}\left[p'(x,t)\right] = \hat{p}(x,s), \tag{A.1}$$

where

$$\hat{p}(x,s) = \int_{t=0}^{\infty} p'(x,t)\,\mathrm{e}^{-st}\mathrm{d}t\,,$$

$$\mathcal{L}\left[\frac{\partial^2 p'}{\partial t^2}\right] = s^2\,\hat{p}(x,s) - \left[s\,p'(x,t) + \dot{p}'(x,t)\right]_{t=0}\,, \tag{A.2}$$

$$\mathcal{L}\left[\frac{\partial q'}{\partial t}\right] = s\,\hat{q}(x,s)\,, \tag{A.3}$$

assuming

$$q'(x,t)|_{t=0} = 0\,,$$

$$\mathcal{L}\left[G_p(x,x^*,t-t^*)\right] = \mathrm{e}^{-st^*}\,\hat{G}_p(x,x^*,s)\,, \tag{A.4}$$

where

$$\hat{G}_p(x,x^*,s) = \int_{t=0}^{\infty} G_p(x,x^*,t-t^*)\,\mathrm{e}^{-s(t-t^*)}\,\mathrm{d}t\,,$$

$$\mathcal{L}\left[\frac{\partial^2 G_p(x,x^*,t-t^*)}{\partial t^2}\right] = s^2\,\mathrm{e}^{-st^*}\hat{G}_p(x,x^*,s), \tag{A.5}$$

given that terms at $t = 0$ are zero due to the causality of the Green's function,

$$\mathcal{L}\left[\delta(t-t^*)\right] = \mathrm{e}^{-st^*}. \tag{A.6}$$

The transformed versions of Eqs. (2.4) and (4.1) are

$$\frac{s^2}{c^2}\hat{G}_p - \frac{\partial^2 \hat{G}_p}{\partial x^2} = \delta(x-x^*) \quad | \cdot\ \hat{p}(x,s) \tag{A.7}$$

$$\frac{s^2}{c^2}\,\hat{p} - \frac{\partial^2 \hat{p}}{\partial x^2} - \frac{1}{c^2}\left[sp'(x,t) + \dot{p}'(x,t)\right]_{t=0} = B\,s\,\hat{q} - \frac{\partial \hat{f}}{\partial x} \quad | \cdot\ \hat{G}_p(x,x^*,s) \tag{A.8}$$

We multiply the equations as indicated (by the notation |.) and subtract Eq. (A.8) from Eq. (A.7). This gives

$$-\hat{p}\frac{\partial^2 \hat{G}_p}{\partial x^2} + \hat{G}_p\frac{\partial^2 \hat{p}}{\partial x^2} + \frac{1}{c^2}[sp'(x,t) + \dot{p}'(x,t)]_{t=0}\hat{G}_p = \hat{p}\,\delta(x-x^*) - B\,s\,\hat{q}\,\hat{G}_p + \frac{\partial \hat{f}}{\partial x}\hat{G}_p\,. \tag{A.9}$$

Next we swap the positions x and x^*, and apply the integral $\int_{x^*=0}^{L}\cdots\,\mathrm{d}x^*$ on both sides of Eq. (A.9). This leads to

$$\underbrace{\int_{x^*=0}^{L}\left(\hat{G}_p\frac{\partial^2 \hat{p}}{\partial x^{*2}} - \hat{p}\frac{\partial^2 \hat{G}_p}{\partial x^{*2}}\right)\mathrm{d}x^*}_{=I_1} + \frac{1}{c^2}\underbrace{\int_{x^*=0}^{L}\left[sp'(x^*,t) + \dot{p}'(x^*,t)\right]_{t=0}\hat{G}_p\mathrm{d}x^*}_{=I_2}$$
$$= \hat{p}(x,s) - B\underbrace{\int_{x^*=0}^{L} s\,\hat{q}(x^*,s)\,\hat{G}_p(x,x^*,s)\,\mathrm{d}x^*}_{=I_3} + \underbrace{\int_{x^*=0}^{L}\frac{\partial \hat{f}}{\partial x^*}\hat{G}_p(x,x^*,s)\,\mathrm{d}x^*}_{=I_4} \tag{A.10}$$

The integrals denoted by I_1, I_2, I_3, I_4 can be simplified, using integration by parts:

$$I_1 = \int_{x^*=0}^{L}\left(\hat{G}_p\frac{\partial^2 \hat{p}}{\partial x^{*2}} - \hat{p}\frac{\partial^2 \hat{G}_p}{\partial x^{*2}}\right)\mathrm{d}x^*$$
$$= \underbrace{\left[\hat{G}_p\frac{\partial \hat{p}}{\partial x^*} - \hat{p}\frac{\partial \hat{G}_p}{\partial x^*}\right]_{x^*=0}^{L}}_{\substack{\text{determined by the}\\ \text{boundary conditions}}} - \underbrace{\int_{x^*=0}^{L}\left(\frac{\partial \hat{G}_p}{\partial x^*}\frac{\partial \hat{p}}{\partial x^*} - \frac{\partial \hat{p}}{\partial x^*}\frac{\partial \hat{G}_p}{\partial x^*}\right)\mathrm{d}x^*}_{=0}\,. \tag{A.11}$$

For the boundary conditions given by Eq. (2.2), the result is clearly

$$I_1 = 0\,. \tag{A.12}$$

It can be shown, by the way, that $I_1 = 0$ is true for many other boundary conditions, e.g. for duct ends described by a frequency-dependent reflection coefficient; this is because $\hat{G}_p$ and $\hat{p}$ satisfy the same boundary conditions.

The integral I_2 is determined by the initial conditions. We assume that they are given by

$$p'(x,t)|_{t=0} = p_0\,\delta(x - x_d)\,, \tag{A.13a}$$

$$\dot{p}'(x,t)|_{t=0} = 0\,, \tag{A.13b}$$

which describe an initial pressure concentrated at the point x_d with magnitude p_0. I_2 then reduces to

$$I_2 = \int_{x^*=0}^{L} s\,p_0 \delta(x^* - x_d)\,\hat{G}_p\,\mathrm{d}x^* = s\,p_0\,\hat{G}_p(x, x_d, s)\,. \tag{A.14}$$

I_3 and I_4 can be simplified with the assumption that the source is compact and located at x_q, as described by Eqs. (3.6) and (3.10). In the s-domain these expressions become

$$\hat{q}(x^*, s) = \hat{Q}(s)\,\delta(x^* - x_q)\,, \tag{A.15}$$

$$\hat{f}(x^*, s) = \hat{F}(s)\,\delta(x^* - x_q)\,. \tag{A.16}$$

Then

$$I_3 = \int_{x^*=0}^{L} s\,\hat{Q}(s)\delta(x^* - x_q)\,\hat{G}_p(x, x^*, s)\,\mathrm{d}x^* = \hat{G}_p(x, x^*, s)\Big|_{x^*=x_q}\,s\,\hat{Q}(s)\,, \tag{A.17}$$

$$\begin{aligned} I_4 &= \int_{x^*=0}^{L} \frac{\partial \hat{f}}{\partial x^*}\,\hat{G}_p\,\mathrm{d}x^* = \underbrace{\left[\hat{f}\,\hat{G}_p\right]_{x^*=0}^{L}}_{\substack{=0 \text{ because} \\ \hat{f}=0 \text{ at } x^*=0,L}} - \int_{x^*=0}^{L} \hat{f}\,\frac{\partial \hat{G}_p}{\partial x^*}\,\mathrm{d}x^* \\ &= -\int_{x^*=0}^{L} \hat{F}\,\delta(x^* - x_q)\,\frac{\partial \hat{G}_p}{\partial x^*}\,\mathrm{d}x^* = -\left.\frac{\partial \hat{G}_p}{\partial x^*}\right|_{x^*=x_q}\hat{F}(s)\,. \end{aligned} \tag{A.18}$$

Eq. (A.10) then becomes

$$\hat{p}(x,s) = B\,\hat{G}_p(x, x_q, s)\,s\,\hat{Q}(s) + \left.\frac{\partial \hat{G}_p}{\partial x^*}\right|_{x^*=x_q}\hat{F}(s) + \frac{1}{c^2}\,p_0\,s\,\hat{G}(x, x_d, s) \tag{A.19}$$

In order to transform this back into the time-domain, we apply the inverse Laplace transform on both sides of Eq. (A.19), using:

$$\mathcal{L}^{-1}\left[\hat{p}(x,s)\right] = p'(x,t)\,, \tag{A.20}$$

$$\begin{aligned} \mathcal{L}^{-1}\left[\hat{G}_p|_{x^*=x_q}\,s\,\hat{Q}(s)\right] &= \int_{t^*=0}^{t} G_p(x, x^*, t - t^*)|_{x^*=x_q}\,\frac{\partial Q'^{\,*}}{\partial t}\,\mathrm{d}t^* \\ &= -\int_{t^*=0}^{t} \left.\frac{\partial G_p(x, x^*, t - t^*)}{\partial t^*}\right|_{x^*=x_q} Q'(t^*)\,\mathrm{d}t^*\,, \end{aligned} \tag{A.21}$$

$$\mathcal{L}^{-1}\left[\left.\frac{\partial \hat{G}_p}{\partial x}^{*}\right|_{x^*=x_q}\hat{F}(s)\right] = \int_{t^*=0}^{t} \left.\frac{\partial G_p(x, x^*, t - t^*)}{\partial x^*}\right|_{x^*=x_q} F'(t^*)\,\mathrm{d}t^*\,, \tag{A.22}$$

$$\mathcal{L}^{-1}\left[s\,\hat{G}_p(x, x_d, s)\right] = \left.\frac{\partial G_p(x, x^*, t)}{\partial t}\right|_{x^*=x_d}\,. \tag{A.23}$$

This leads to

$$\begin{aligned} p'(x,t) = &- B\int_{t^*=0}^{t} \left.\frac{\partial G_p(x, x^*, t - t^*)}{\partial t^*}\right|_{x^*=x_q} Q'(t^*)\,\mathrm{d}t^* \\ &+ \int_{t^*=0}^{t} \left.\frac{\partial G_p(x, x^*, t - t^*)}{\partial x^*}\right|_{x^*=x_q} F'(t^*)\,\mathrm{d}t^* + \frac{p_0}{c^2}\left.\frac{\partial G_p(x, x^*, t)}{\partial t}\right|_{x^*=x_d}\,. \end{aligned} \tag{A.24}$$

There are three terms on the right-hand side of Eq. (A.24): the first term represents the feedback between the acoustic field and the heat release rate $Q'(t)$; the second term represents the feedback between the acoustic field and the dipole force $F'(t)$; the third term represents the free oscillation, which is triggered by the initial pressure p_0. We omit the third term in this paper because

it would interfere with the feedback between the acoustic field and the two sources. This would add unnecessary complications to understanding our time histories. Instead, we kick-start the acoustic field in the first iteration step in such a way that the free oscillation is suppressed.

The integral equation for the *velocity* is derived in much the same way as that for the pressure. The starting point are the two governing PDEs for G_u (see Eq. (2.4)) and u' (see Eq. (4.3)). They are manipulated by the same steps shown for the pressure in Eqs. (A.1)–(A.10). The integral equivalent to I_2 is determined by the initial conditions for the velocity. We assume

$$u'(x,t)|_{t=0} = u_0\,\delta(x-x_d)\,, \tag{A.25a}$$

$$\dot{u}'(x,t)|_{t=0} = 0\,, \tag{A.25b}$$

which represents an initial velocity concentrated at the point x_d with magnitude u_0. The subsequent manipulations are directly analogous to those given in Eqs. (A.14)–(A.23). The final result is

$$\begin{aligned} u'(x,t) = &\frac{B}{\bar{\rho}} \int_{t^*=0}^{t} \left.\frac{\partial G_u(x,x^*,t-t^*)}{\partial x^*}\right|_{x^*=x_q} Q'(t^*)\,\mathrm{d}t^* \\ &- \frac{1}{\bar{\rho}\,c^2} \int_{t^*=0}^{t} \left.\frac{\partial G_u(x,x^*,t-t^*)}{\partial t^*}\right|_{x^*=x_q} F'(t^*)\,\mathrm{d}t^* + \frac{u_0}{c^2} \left.\frac{\partial G_u(x,x^*,t)}{\partial t}\right|_{x^*=x_d}\,. \end{aligned} \tag{A.26}$$

Appendix B. Iteration scheme for sources described in the time-domain

We write the Green's functions G_p and G_u (see Eqs. (2.5), (2.6)) in compact form,

$$G_p(x,x^*,t-t^*) = \sum_{n=1}^{\infty} g_{pn}(x,x^*)\sin\omega_n(t-t^*)\,, \tag{B.1}$$

$$G_u(x,x^*,t-t^*) = \sum_{n=1}^{\infty} g_{un}(x,x^*)\sin\omega_n(t-t^*)\,, \tag{B.2}$$

having introduced the abbreviations

$$g_{pn}(x,x^*) = \begin{cases} \dfrac{2c}{\pi}\dfrac{(-1)^n}{n}\sin\dfrac{\omega_n x}{c}\sin\dfrac{\omega_n(x^*-L)}{c} & \text{for } x<x^* \\ \dfrac{2c}{\pi}\dfrac{(-1)^n}{n}\sin\dfrac{\omega_n (x-L)}{c}\sin\dfrac{\omega_n x^*}{c} & \text{for } x>x^* \end{cases} \tag{B.3}$$

and

$$g_{un}(x,x^*) = \begin{cases} \dfrac{2c}{\pi}\dfrac{(-1)^n}{n}\cos\dfrac{\omega_n x}{c}\cos\dfrac{\omega_n(x^*-L)}{c} & \text{for } x<x^* \\ \dfrac{2c}{\pi}\dfrac{(-1)^n}{n}\cos\dfrac{\omega_n (x-L)}{c}\cos\dfrac{\omega_n x^*}{c} & \text{for } x>x^* \end{cases} \tag{B.4}$$

Also, we have omitted spelling out the Heaviside functions $H(t-t^*)$ in Eqs. (B.1) and (B.2) because they reduce to factors 1 in the integration range $t^*=0,\,\ldots,\,t$.

Then the Green's function derivatives required in Eqs. (4.5) and (4.6) can be written as

$$\frac{\partial G_p}{\partial x^*} = \sum_{n=1}^{\infty} \frac{\partial g_{pn}(x,x^*)}{\partial x^*}(-\mathrm{Im}[\mathrm{e}^{-\mathrm{i}\omega_n(t-t^*)}])\,, \tag{B.5}$$

$$\frac{\partial G_p}{\partial t^*} = \sum_{n=1}^{\infty} g_{pn}(x,x^*)(-\omega_n)(\mathrm{Re}[\mathrm{e}^{-\mathrm{i}\omega_n(t-t^*)}])\,, \tag{B.6}$$

$$\frac{\partial G_u}{\partial x^*} = \sum_{n=1}^{\infty} \frac{\partial g_{un}(x,x^*)}{\partial x^*}(-\mathrm{Im}[\mathrm{e}^{-\mathrm{i}\omega_n(t-t^*)}])\,, \tag{B.7}$$

$$\frac{\partial G_u}{\partial t^*} = \sum_{n=1}^{\infty} g_{un}(x,x^*)(-\omega_n)(\mathrm{Re}[\mathrm{e}^{-\mathrm{i}\omega_n(t-t^*)}])\,, \tag{B.8}$$

After inserting Eqs. (B.5) to (B.8) into the integral Eqs. (4.5) and (4.6), we obtain

$$\begin{aligned} p_1'(t) = &-B\sum_n g_{pn}(x,x^*)\Big|_{\substack{x=x_q\\x^*=x_q}}(-\omega_n)\,\mathrm{Re}\left[\mathrm{e}^{-\mathrm{i}\omega_n t}\underbrace{\int_{t^*=0}^{t}\mathrm{e}^{\mathrm{i}\omega_n t^*}Q'(t^*)\,\mathrm{d}t^*}_{=I_{qn}(t)}\right] \\ &+\sum_n \left.\frac{\partial g_{pn}(x,x^*)}{\partial x^*}\right|_{\substack{x=x_q\\x^*=x_q}}\mathrm{Im}\left[-\mathrm{e}^{-\mathrm{i}\omega_n t}\underbrace{\int_{t^*=0}^{t}\mathrm{e}^{\mathrm{i}\omega_n t^*}F'(t^*)\,\mathrm{d}t^*}_{=I_{fn}(t)}\right] \end{aligned} \tag{B.9}$$

and

$$u_1'(t) = \frac{B}{\bar{\rho}} \sum_n \left. \frac{\partial g_{un}(x,x^*)}{\partial x^*} \right|_{\substack{x=x_q \\ x^*=x_q}} \mathrm{Im}\left[-\mathrm{e}^{-\mathrm{i}\omega_n t} \underbrace{\int_{t^*=0}^{t} \mathrm{e}^{\mathrm{i}\omega_n t^*} Q'(t^*)\,\mathrm{d}t^*}_{=I_{qn}(t)} \right]$$
$$- \frac{1}{\bar{\rho}\, c^2} \sum_n g_{un}(x,x^*)\Big|_{\substack{x=x_q \\ x^*=x_q}} (-\omega_n)\,\mathrm{Re}\left[\mathrm{e}^{-\mathrm{i}\omega_n t} \underbrace{\int_{t^*=0}^{t} \mathrm{e}^{\mathrm{i}\omega_n t^*} F'(t^*)\,\mathrm{d}t^*}_{=I_{fn}(t)} \right]. \tag{B.10}$$

The quantities to be updated in every time step are $Q'(t)$, $F'(t)$, $I_{qn}(t)$, $I_{fn}(t)$, $p_1'(t)$ and $u_1'(t)$.

The two newly introduced integrals, $I_{qn}(t)$ and $I_{fn}(t)$, have the same integration range, $t^* = 0, \ldots, t$. We update them by dividing the integration range for $I_{qn}(t+\Delta t)$ and $I_{fn}(t+\Delta t)$ into two parts: the first part is the interval $t^* = 0, \ldots, t$, and the second part is the short time interval $t^* = t, \ldots, t+\Delta t$. For I_{qn} we then get

$$I_{qn}(t+\Delta t) = \int_{t^*=0}^{t} \mathrm{e}^{\mathrm{i}\omega_n t^*} Q'(t^*)\,\mathrm{d}t^* + \int_{t^*=t}^{t+\Delta t} \mathrm{e}^{\mathrm{i}\omega_n t^*} Q'(t^*)\,\mathrm{d}t^*\,. \tag{B.11}$$

The first integral represents $I_{qn}(t)$. The second integral can be approximated: the time interval Δt is assumed to be very small (compared with an oscillation period of the highest mode of interest), and therefore the source term Q' is nearly constant in this interval and approximately equal to $Q'(t)$. With this rationale, Eq. (B.11) can be written as

$$I_{qn}(t+\Delta t) = I_{qn}(t) + Q'(t)\,\frac{\mathrm{e}^{\mathrm{i}\omega_n t}}{\mathrm{i}\,\omega_n}\left(\mathrm{e}^{\mathrm{i}\omega_n \Delta t} - 1\right), \tag{B.12}$$

and an analogous result is obtained for $I_{fn}(t)$,

$$I_{fn}(t+\Delta t) = I_{fn}(t) + F'(t)\,\frac{\mathrm{e}^{\mathrm{i}\omega_n t}}{\mathrm{i}\,\omega_n}\left(\mathrm{e}^{\mathrm{i}\omega_n \Delta t} - 1\right), \tag{B.13}$$

This leads with Eqs. (B.9) and (B.10) to

$$p_1'(t+\Delta t) = B \sum_n g_{pn}(x,x^*)\Big|_{\substack{x=x_q \\ x^*=x_q}} \omega_n\,\mathrm{Re}\left[\mathrm{e}^{-\mathrm{i}\omega_n(t+\Delta t)} I_{qn}(t+\Delta t)\right]$$
$$+ \sum_n \left. \frac{\partial g_{pn}(x,x^*)}{\partial x^*} \right|_{\substack{x=x_q \\ x^*=x_q}} \mathrm{Im}\left[-\mathrm{e}^{-\mathrm{i}\omega_n(t+\Delta t)} I_{fn}(t+\Delta t)\right] \tag{B.14}$$

and

$$u_1'(t+\Delta t) = \frac{B}{\bar{\rho}} \sum_n \left. \frac{\partial g_{un}(x,x^*)}{\partial x^*} \right|_{\substack{x=x_q \\ x^*=x_q}} \mathrm{Im}\left[-\mathrm{e}^{-\mathrm{i}\omega_n(t+\Delta t)} I_{qn}(t+\Delta t)\right]$$
$$+ \frac{1}{\bar{\rho}\, c^2} \sum_n g_{un}(x,x^*)\Big|_{\substack{x=x_q \\ x^*=x_q}} \omega_n\,\mathrm{Re}\left[\mathrm{e}^{-\mathrm{i}\omega_n(t+\Delta t)} I_{fn}(t+\Delta t)\right]. \tag{B.15}$$

The iteration is started from initial values, given for example for $Q'(t)|_{t=0}$ or $F'(t)|_{t=0}$.

Appendix C. Iteration scheme for sources described in the frequency-domain

The iteration process described in Appendix B assumes that the source terms Q' and F' are given in the time-domain. However, more often than not, they are given in the frequency-domain. Typical examples are

$$\hat{Q}(\omega) = \mathcal{T}(\omega)\,\hat{u}_1(\omega)\,, \tag{C.1}$$

$$\hat{F}(\omega) = Z(\omega)\,\hat{u}_1(\omega)\,, \tag{C.2}$$

where $\mathcal{T}(\omega)$ is a flame transfer function, and $Z(\omega)$ is a transfer impedance. The time-domain equivalents of $\mathcal{T}(\omega)$ and $Z(\omega)$ are time-lag response functions, which we denote by $\mathcal{T}'(t)$ and $Z'(t)$. They appear in the convolution integrals that arise when Eqs. (C.1) and (C.1) are transformed into the time-domain,

$$Q'(t) = \int_{\tau=0}^{t} \mathcal{T}'(t-\tau)\,u_1'(\tau)\,\mathrm{d}\tau\,, \tag{C.3}$$

$$F'(t) = \int_{\tau=0}^{t} Z'(t-\tau)\,u_1'(\tau)\,\mathrm{d}\tau\,. \tag{C.4}$$

This formulation can be incorporated into the iteration scheme described in Appendix B. We illustrate this for the special case, where a dipole force is present, but no heat source. The integral equation, Eq. (A.26), for the acoustic velocity then reduces to

$$u_1'(t) = -\frac{1}{\bar{\rho}\, c^2} \int_{t^*=0}^{t} \left. \frac{\partial G_u(x, x^*, t-t^*)}{\partial t^*} \right|_{\substack{x=x_q \\ x^*=x_q}} F'(t^*)\, \mathrm{d}t^* \,. \tag{C.5}$$

With the time derivative of the Green's function given by Eq. (B.8), Eq. (C.5) can be written as

$$u_1'(t) = \frac{1}{\bar{\rho}\, c^2} \,\mathrm{Re} \sum_n \left[\underbrace{\int_{t^*=0}^{t} g_{un} \omega_n \, \mathrm{e}^{-\mathrm{i}\omega_n (t-t^*)} F'(t^*)\, \mathrm{d}t^*}_{=I_n(t)} \right] . \tag{C.6}$$

We now need to obtain $F'(t)$ from the frequency-domain formulation $Z(\omega)$. To this end, we approximate $Z(\omega)$ by a series of "basis functions" that can be transformed analytically into the time-domain. A tried and tested series of basis functions are rational functions [40]

$$Z(\omega) \approx \sum_k \frac{b_k}{-\mathrm{i}\omega - a_k} \,, \tag{C.7}$$

where the a_k and b_k are fitting parameters, which are either real or they come in complex conjugate pairs. In our notation, (time dependence $\mathrm{e}^{-\mathrm{i}\omega t}$), all the a_k have positive real parts. The time-domain version of Eq. (C.7) is

$$Z'(t) = \sum_k b_k \, \mathrm{e}^{-a_k t} \,. \tag{C.8}$$

With Eq. (C.4) we get for the dipole force

$$F'(t) = \sum_k \underbrace{\int_{\tau=0}^{t} b_k \, \mathrm{e}^{-a_k (t-\tau)} \, u_1'(\tau)\, \mathrm{d}\tau}_{=F_k(t)} \,, \tag{C.9}$$

where the abbreviation $F_k(t)$ has been introduced as shown just below Eq. (C.9).

The quantities to be updated in every time step are $F_k(t)$, $I_n(t)$ and $u_1'(t)$. In order to update $F_k(t)$ and $I_n(t)$, we adopt the same strategy as in Appendix B, of dividing the integration range for $F_k(t+\Delta t)$ and $I_n(t+\Delta t)$ into two parts: the first part is the interval $t^* = 0, \ldots, t$, and the second part is the short time interval $t^* = t, \ldots, t+\Delta t$. We then get for the force

$$F(t+\Delta t) = \sum_k F_k(t+\Delta t) \,, \tag{C.10}$$

with

$$F_k(t+\Delta t) = \mathrm{e}^{-a_k \Delta t} \, F_k(t) + u_1'(t) \, \frac{b_k}{a_k} \, (1 - \mathrm{e}^{-a_k \Delta t}) \,. \tag{C.11}$$

For the integral $I_n(t+\Delta t)$, we get

$$I_n(t+\Delta t) = \mathrm{e}^{-\mathrm{i}\omega_n \Delta t} \, I_n(t) + F'(t)(-\mathrm{i}) g_{un} (1 - \mathrm{e}^{-\mathrm{i}\omega_n \Delta t}) \,. \tag{C.12}$$

Finally, u_1' is updated by

$$u_1'(t+\Delta t) = \frac{1}{\bar{\rho}\, c^2} \,\mathrm{Re} \sum_n \left[\mathrm{e}^{-\mathrm{i}\omega_n \Delta t} \, I_n(t) + F'(t) \, (-\mathrm{i}) \, g_{un} \, (1 - \mathrm{e}^{-\mathrm{i}\omega_n \Delta t}) \right] . \tag{C.13}$$

Gaussian basis functions are an alternative to rational ones. They are not used in this paper, but could be convenient to approximate flame transfer functions $\mathcal{T}(\omega)$, which are given in the frequency domain. They have been used by Gopinathan et al. [41] to approximate a flame transfer function by

$$\mathcal{T}(\omega) \approx \sum_k n_k \, \mathrm{e}^{\mathrm{i}\omega\tau_k} \, \mathrm{e}^{-0.5\, \omega^2 \sigma_k^2} \,; \tag{C.14}$$

here the fitting parameters are n_k, τ_k and σ_k and they are also determined with a nonlinear least squares routine. The time-domain version of Eq. (C.14) is

$$\mathcal{T}'(t) = \sum_k \frac{n_k}{\sigma_k \sqrt{2\pi}} \, \mathrm{e}^{-\frac{(t-\tau_k)^2}{2\sigma_k^2}} \,. \tag{C.15}$$

Appendix D. Calculation of the tailored Green's function of a duct with open ends

We show this calculation for the *velocity* Green's function G_u, but drop the subscript u here for convenience. Fig. D.1 shows the considered configuration. A uniform duct of length L has open ends and houses a point source at position x^* firing an impulse at time t^*.

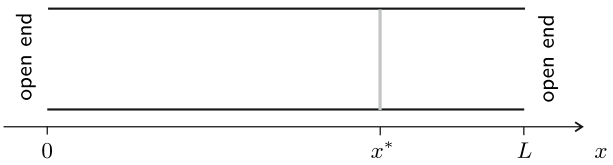

Fig. D.1. Uniform open-ended duct with point source at x^*.

The acoustic velocity field generated by the point source is the required Green's function $G(x, x^*, t - t^*)$. It is described by the PDE Eq. (2.4),

$$\frac{1}{c^2}\frac{\partial^2 G}{\partial t^2} - \frac{\partial^2 G}{\partial x^2} = \delta\left(x - x^*\right)\ \delta\left(t - t^*\right)\,, \tag{D.1}$$

and the boundary conditions for the acoustic velocity Eq. (2.3),

$$\left.\frac{\partial G}{\partial x}\right|_{x=0} = \left.\frac{\partial G}{\partial x}\right|_{x=L} = 0. \tag{D.2}$$

We calculate $G(x, x^*, t - t^*)$ in two steps. In the first step, we will determine its frequency-domain equivalent, which in the second step we will transform into the time-domain.

Frequency-domain Green's function

We denote the frequency-domain Green's function by $\hat{G}(x, x^*, \omega)$. It satisfies the inhomogeneous Helmholtz equation,

$$\frac{\partial^2 \hat{G}}{\partial x^2} + k^2 \hat{G} = \delta(x - x^*) \tag{D.3}$$

and the boundary conditions given in Eq. (D.2). These boundary conditions are satisfied by the following trial solution,

$$\hat{G} = \begin{cases} A\cos kx & \text{for the region} \quad 0 < x < x^* \\ B\cos k(x - L) & \text{for the region} \quad x^* < x < L \end{cases} \tag{D.4}$$

where A and B are functions of x^* which are to be determined. With the Heaviside function H, we can combine the two functions in Eq. (D.4) into a single expression,

$$\hat{G} = AH(x^* - x)\cos kx + BH(x - x^*)\cos k(x - L)\,. \tag{D.5}$$

We will determine A and B by substituting Eq. (D.5) into the PDE Eq. (D.3), noting that differentiation of Eq. (D.5) with respect to x requires the derivative of H, which is a generalised function. This is given by

$$\frac{\partial H(x - x^*)}{\partial x} = \delta(x - x^*) \text{ and } \frac{\partial H(x^* - x)}{\partial x} = -\delta(x - x^*)\,. \tag{D.6a,b}$$

The first and second derivative of Eq. (D.5) can then be written as

$$\begin{aligned}\frac{\partial \hat{G}}{\partial x} =& -A\underbrace{\delta(x - x^*)\cos kx}_{=\delta(x-x^*)\cos kx^*} + B\underbrace{\delta(x - x^*)\cos k(x - L)}_{\delta(x-x^*)\cos k(x^*-L)} \\ &- kAH\,(x^* - x)\sin kx - kBH\,(x - x^*)\sin k(x - L)\end{aligned} \tag{D.7}$$

$$\begin{aligned}\frac{\partial^2 \hat{G}}{\partial x^2} =& -A\,\delta'(x - x^*)\cos kx^* + B\,\delta'(x - x^*)cosk(x^* - L) \\ &+ kA\,\delta(x - x^*)\sin kx^* - kB\,\delta(x - x^*)\sin k(x^* - L) \\ &\underbrace{-k^2 A\,H(x^* - x)\cos kx - k^2 B\,H(x - x^*)\cos k(x - L)}_{=-k^2\hat{G}}\end{aligned} \tag{D.8}$$

Note that in Eq. (D.7) we have made use of the fact that a function $\varphi(x)$ loses its x-dependence when multiplied by the delta-function,

$$\varphi(x)\,\delta(x - x^*) = \varphi(x^*)\,\delta(x - x^*). \tag{D.9}$$

Substitution of Eq. (D.8) into Eq. (D.3) leads to

$$\delta'(x - x^*)\left[-A\cos kx^* + B\cos k(x^* - L)\right] + \delta(x - x^*)\,k\left[A\sin kx^* - B\sin k(x^* - L)\right] = \delta(x - x^*)\,. \tag{D.10}$$

We extract two equations from Eq. (D.10) by comparing the coefficients of $\delta(x - x^*)$ and $\delta'(x - x^*)$,

$$-A\cos kx^* + B\cos k(x^* - L) = 0\,, \tag{D.11a}$$

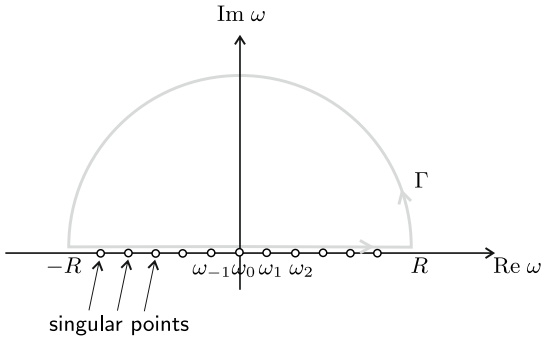

Fig. D.2. Singular points and integration path in the complex ω plane for $t < t^*$.

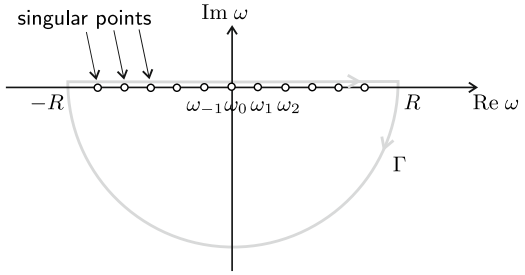

Fig. D.3. Singular points and integration path in the complex ω plane for $t > t^*$.

$$A \sin kx^* - B \sin k(x^* - L) = \frac{1}{k}\,. \tag{D.11b}$$

These are linear equations for A and B, and the solutions are

$$A = \frac{\cos k(x^* - L)}{k \sin kL}\,, \tag{D.12a}$$

$$B = \frac{\cos kx^*}{k \sin kL}\,, \tag{D.12b}$$

(where $\sin kx^* \cos k(x^* - L) - \cos kx^* \sin k(x^* - L) = \sin kL$ has been used). Substitution of Eq. (D.12) into Eq. (D.4) gives

$$\hat{G}(x, x^*, \omega) = \begin{cases} \dfrac{\cos kx \cos k(x^* - L)}{k \sin kL} & \text{for the region } \; 0 < x < x^* \\ \dfrac{\cos k(x - L) \cos kx^*}{k \sin kL} & \text{for the region } \; x^* < x < L \end{cases} \tag{D.13a,b}$$

This function is continuous across $x = x^*$, but its gradient, $\frac{\partial \hat{G}}{\partial x}$ jumps by 1.

Time-domain Green's function

The time-domain Green's function is the inverse Fourier transform of the frequency-domain Green's function,

$$G(x, x^*, t - t^*) = -\frac{1}{2\pi} \int_{-\infty}^{\infty} \hat{G}(x, x^*, \omega)\, \mathrm{e}^{-\mathrm{i}\omega(t - t^*)}\, \mathrm{d}\omega\,, \tag{D.14}$$

and can be calculated with the residue theorem. The integrand in Eq. (D.14) has infinitely many singular points along the real axis; those at $\omega_n = \frac{n\pi c}{L}$ with $n = \pm 1,\ \pm 2\,, \pm 3,\ \ldots$ are simple poles, and at $\omega_0 = 0$ there is a pole of order 2.

The time-domain Green's function needs to be causal, i.e. $G = 0$ for $t - t^* < 0$ (before the impact) and $G \neq 0$ for $t - t^* > 0$ (after the impact). We satisfy this by a suitable choice of the integration path in the complex ω plane when applying the residue theorem. The path for $t - t^* < 0$ is shown in Fig. D.2, and that for $t - t^* > 0$ in Fig. D.3.

Before the impact ($t < t^*$)

There are no singular points enclosed by the integration path, and the integral along the semicircular arc Γ can be shown to vanish as $R \to \infty$; therefore

$$G(x, x^*, t - t^*) = 0 \quad \text{for} \quad t < t^*\,. \tag{D.15}$$

After the impact ($t > t^*$)

Again, the integral along the semicircular arc Γ can be shown to vanish as $R \to \infty$. According to the residue theorem (note that the integration path is traversed in the clockwise, i.e. negative, direction),

$$G(x, x^*, t - t^*) = -\frac{1}{2\pi}(-2\pi \mathrm{i}) \sum_{n=-\infty}^{\infty} \mathrm{Res}_{\omega_n} \left[\hat{G}(x, x^*, \omega)\, \mathrm{e}^{-\mathrm{i}\omega(t-t^*)} \right] . \tag{D.16}$$

Calculation of residues

At the pole ω_0, the residue can be calculated by constructing the Laurent series expansion of $\hat{G}(x, x^*, \omega)\, \mathrm{e}^{-\mathrm{i}\omega(t-t^*)}$ with respect to ω. It turns out that there is no term of order ω^{-1} in the expansion, and therefore

$$\mathrm{Res}_{\omega_0} \hat{G}(x, x^*, \omega)\, \mathrm{e}^{-\mathrm{i}\omega(t-t^*)} = 0 . \tag{D.17}$$

At the simple poles ω_n with $n \neq 0$, the residue can be calculated with the following formula, for two analytical functions $P(\omega)$ and $Q(\omega)$,

$$\mathrm{Res}_{\omega_n} \left[\frac{P(\omega)}{Q(\omega)} \right] = \frac{P(\omega_n)}{Q'(\omega_n)} . \tag{D.18}$$

For the region $0 < x < x^*$ (see Eq. ((D.13)a), with $k = \frac{\omega}{c}$),

$$P(\omega) = \cos\frac{\omega x}{c} \cos\frac{\omega(x^* - L)}{c}\, \mathrm{e}^{-\mathrm{i}\omega(t-t^*)} , \tag{D.19}$$

$$Q(\omega) = \frac{\omega}{c} \sin\frac{\omega L}{c} \quad \Rightarrow \quad Q'(\omega) = \frac{1}{c}\left[\sin\frac{\omega L}{c} + \frac{\omega L}{c} \cos\frac{\omega L}{c} \right] , \tag{D.20}$$

and with $\omega_n = \frac{n\pi c}{L}$,

$$Q'(\omega_n) = \frac{(-1)^n n\pi}{c} . \tag{D.21}$$

Then Eq. (D.16) becomes

$$\mathrm{Res}_{\omega_n} \left[\hat{G}(x, x^*, \omega)\, \mathrm{e}^{-\mathrm{i}\omega(t-t^*)} \right] = (-1)^n \frac{c}{n\pi} \cos\frac{\omega_n x}{c} \cos\frac{\omega_n(x^* - L)}{c}\, \mathrm{e}^{-\mathrm{i}\omega_n(t-t^*)} . \tag{D.22}$$

This is for the region $0 < x < x^*$.

For the region $x^* < x < L$, the residue is obtained in the same way resulting in (x and x^* swapped over)

$$\mathrm{Res}_{\omega_n} \left[\hat{G}(x, x^*, \omega)\, \mathrm{e}^{-\mathrm{i}\omega(t-t^*)} \right] = (-1)^n \frac{c}{n\pi} \cos\frac{\omega_n(x - L)}{c} \cos\frac{\omega_n x^*}{c}\, \mathrm{e}^{-\mathrm{i}\omega_n(t-t^*)} . \tag{D.23}$$

The sum in Eq. (D.16) includes positive and negative mode numbers. It can be reduced to a sum over only positive mode numbers by using $\omega_{-n} = -\omega_n$.

Final result for the velocity Green's function

The results for before and after the impact can be combined with the Heaviside function,

$$H(t - t^*) = \begin{cases} 0 & \text{if} \quad t < t^* \\ 1 & \text{if} \quad t > t^* \end{cases} \tag{D.24}$$

to give

$$G(x, x^*, t - t^*) = \begin{cases} H(t - t^*)\, \dfrac{2c}{\pi} \displaystyle\sum_{n=1}^{\infty} \dfrac{(-1)^n}{n} \cos\dfrac{\omega_n x}{c} \cos\dfrac{\omega_n(x^* - L)}{c} \sin\omega_n(t - t^*) & \text{for} \quad 0 < x < x^* \\ H(t - t^*)\, \dfrac{2c}{\pi} \displaystyle\sum_{n=1}^{\infty} \dfrac{(-1)^n}{n} \cos\dfrac{\omega_n(x - L)}{c} \cos\dfrac{\omega_n x^*}{c} \sin\omega_n(t - t^*) & \text{for} \quad x^* < x < L \end{cases} \tag{D.25}$$

G is an impulse response and behaves as expected: it is zero before the impulse (until $t = t^*$), and a superposition of modes thereafter. These modes have the same frequencies as the eigenmodes of the duct, however, they are *not* the eigenmodes because their spatial distribution has a singularity at $x = x^*$. Also, the Green's function in (D.25) satisfies reciprocity, i.e. it does not change if x and x^* are swapped over.

Tailored Green's function for the pressure

The Green's function for the pressure, $G_p(x, x^*, t - t^*)$, needs to satisfy the pressure boundary conditions Eq. (2.2), and this requires the following trial solution instead of Eq. (D.4),

$$\hat{G} = \begin{cases} A \sin kx & \text{for the region} \quad 0 < x < x^* \\ B \sin k(x - L) & \text{for the region} \quad x^* < x < L \end{cases} \tag{D.26}$$

Otherwise, the Green's function for the pressure is calculated by the same method as that shown above for the velocity. The result is given in Eq. (2.5).

References

[1] D.G. Crighton, A.P. Dowling, J.E. Ffowcs Williams, M. Heckl, F.G. Leppington, Modern Methods in Analytical Acoustics, Springer-Verlag, London, 1992.
[2] L. Challis, F. Sheard, The Green of Green functions, Phys. Today 56 (12) (2003) 41–46, http://dx.doi.org/10.1063/1.1650227.
[3] M. Lighthill, On sound generated aerodynamically I. General theory, Proc. R. Soc. Lond. A 211 (1107) (1952) 564–587, http://dx.doi.org/10.1098/rspa.1952.0060.
[4] M. Lighthill, On sound generated aerodynamically II. Turbulence as a source of sound, Proc. R. Soc. Lond. A 222 (1148) (1954) 1–32, http://dx.doi.org/10.1098/rspa.1954.0049.
[5] A. Hirschberg, S.W. Rienstra, An introduction to aeroacoustics, Technical Report Version:18-07-2004, Technische Universiteit Eindhoven, 2004, URL: https://www.win.tue.nl/sjoerdr/papers/les-swr-mh.pdf.
[6] A. Hirschberg, C. Schram, A primitive approach to aeroacoustics, in: Y. Aurégan, V. Pagneux, J.F. Pinton, A. Maurel (Eds.), Sound-Flow Interactions Lecture Notes in Physics, Springer Berlin Heidelberg, 2002, pp. 1–30, http://dx.doi.org/10.1007/3-540-45880-8_1.
[7] P. Doak, Acoustic radiation from a turbulent fluid containing foreign bodies, Proc. R. Soc. Lond. A 254 (1276) (1960) 129–145, http://dx.doi.org/10.1098/rspa.1960.0010.
[8] J.E. Ffowcs Williams, L.H. Hall, Aerodynamic sound generation by turbulent flow in the vicinity of a scattering half plane, J. Fluid Mech. 40 (04) (1970) 657–670, http://dx.doi.org/10.1017/s0022112070000368.
[9] M. Howe, Edge-source acoustic Green's function for an airfoil of arbitrary chord, with application to trailing-edge noise, Quart. J. Mech. Appl. Math. 54 (1) (2001) 139–155, http://dx.doi.org/10.1093/qjmam/54.1.139.
[10] M. Roger, On combined propeller synchronisation and edge scattering for the noise reduction of distributed propulsion systems, in: Proceedings of the 26th International Congress on Sound and Vibration, Montreal, Canada, 2019.
[11] M. Howe, The generation of sound by aerodynamic sources in an inhomogeneous steady flow, J. Fluid Mech. 67 (3) (1975) 597–610, http://dx.doi.org/10.1017/s0022112075000493.
[12] J.E. Ffowcs Williams, M.S. Howe, The generation of sound by density inhomogeneities in low Mach number nozzle flows, J. Fluid Mech. 70 (3) (1975) 605–622, http://dx.doi.org/10.1017/s0022112075002224.
[13] M. Howe, The compression wave produced by a high-speed train entering a tunnel, Proc. R. Soc. Lond. A 454 (1974) (1998) 1523–1534, http://dx.doi.org/10.1098/rspa.1998.0220.
[14] M.S. Howe, R.S. McGowan, Production of sound by unsteady throttling of flow into a resonant cavity, with application to voiced speech, J. Fluid Mech. 672 (2011) 428–450, http://dx.doi.org/10.1017/s0022112010006117.
[15] P.M. Morse, H. Feshbach, Methods of Theoretical Physics. Part 1, McGraw-Hill, New York, 1953.
[16] P.M. Morse, U. Ingard, Theoretical Acoustics, Princeton University Press, Princeton, 1986.
[17] P. Doak, Excitation, transmission and radiation of sound from source distributions in hard-walled ducts of finite length (I): The effects of duct cross-section geometry and source distribution space-time pattern, J. Sound Vib. 31 (1) (1973) 1–72, http://dx.doi.org/10.1016/s0022-460x(73)80249-4.
[18] P. Doak, Excitation, transmission and radiation of sound from source distributions in hard-walled ducts of finite length (II): The effects of duct length, J. Sound Vib. 31 (2) (1973) 137–174, http://dx.doi.org/10.1016/s0022-460x(73)80372-4.
[19] S.-W. Kang, Y.-H. Kim, Green function analysis of the acoustic field in a finite three-port circular chamber, J. Sound Vib. 181 (5) (1995) 765–780, http://dx.doi.org/10.1006/jsvi.1995.0170.
[20] D. Veerababu, B. Venkatesham, Three-dimensional acoustic analysis of concentric tube resonator using Green's function, in: Proceedings of the 24th International Congress on Sound and Vibration, London, UK, 23-27 July 2017.
[21] M.A. Heckl, M.S. Howe, Stability analysis of the Rijke tube with a Green's function approach, J. Sound Vib. 305 (4–5) (2007) 672–688, http://dx.doi.org/10.1016/j.jsv.2007.04.027.
[22] M.A. Heckl, Active control of the noise from a Rijke tube, J. Sound Vib. 124 (1) (1988) 117–133, http://dx.doi.org/10.1016/s0022-460x(88)81408-1.
[23] R.L. Raun, M.W. Beckstead, J.C. Finlinson, K.P. Brooks, A review of Rijke tubes, Rijke burners and related devices, Prog. Energ. Combust. 19 (4) (1993) 313–364, http://dx.doi.org/10.1016/0360-1285(93)90007-2.
[24] A. Hirschberg, Introduction to aero-acoustics of internal flows, in: Advances in Aeroacoustics, Van Karman Institute for Fluid Dynamics, Rhode-St-Genèse, Belguim, 2009, pp. 1–112.
[25] A. Bigongiari, M.A. Heckl, A Green's function approach to the rapid prediction of thermoacoustic instabilities in combustors, J. Fluid Mech. 798 (2016) 970–996, http://dx.doi.org/10.1017/jfm.2016.332.
[26] X. Wang, M. Heckl, 3-D thermoacoustic instability analysis based on Green's function approach, J. Sound Vib. (2022) 116816, http://dx.doi.org/10.1016/j.jsv.2022.116816.
[27] J. Su, D. Yang, A.S. Morgans, Modelling of sound-vortex interaction for the flow through an annular aperture, J. Sound Vib. 509 (2021) 116250, http://dx.doi.org/10.1016/j.jsv.2021.116250.
[28] S.W. Rienstra, A. Hirschberg, An Introduction to Acoustics, Technical Report IWDE 92-06, revised, Technische Universiteit Eindhoven, 2009, URL: https://b-k.cc/book/3049378/185c6e.
[29] A.P. Dowling, J.E. Ffowcs Williams, Sound and Sources of Sound, Ellis Horwood, Chichester, 1983.
[30] M. Munjal, Acoustics of Ducts and Mufflers, John Wiley & Sons, New York, 1987.
[31] K. Yamamoto, A. Müller, T. Ashida, K. Yonezawa, F. Avellan, Y. Tsujimoto, Experimental method for the evaluation of the dynamic transfer matrix using pressure transducers, J. Hydraul. Res. 53 (4) (2015) 466–477, http://dx.doi.org/10.1080/00221686.2015.1050076.
[32] C.O. Paschereit, B. Schuermans, W. Polifke, O. Mattson, Measurement of transfer matrices and source terms of premixed flames, J. Eng. Gas Turbines Power 124 (2) (2002) 239–247, http://dx.doi.org/10.1115/1.1383255.
[33] F. Tricomi, Integral Equations, Re-Issued 1985, Dover Publications, New York, 1957.
[34] N. Ananthakrishnan, S. Deo, F.E.C. Culick, Reduced-order modeling and dynamics of nonlinear acoustic waves in a combustion chamber, Combust. Sci. Technol. 177 (2) (2005) 221–247, http://dx.doi.org/10.1080/00102200590900219.
[35] B.T. Zinn, M.E. Lores, Application of the Galerkin method in the solution of non-linear axial combustion instability problems in liquid rockets, Combust. Sci. Technol. 4 (1) (1972) 269–278, http://dx.doi.org/10.1080/00102207108952493.
[36] F. Culick, Combustion Instabilities in Solid Propellant Rocket Motors, Lectures Presented at the RTO/VKI Special Course on "Internal Aerodynamics in Solid Rocket Propulsion", NATO Technical Report, RTO-EN-023, held in Rhode-Saint-Genèse, Belgium, 2002.
[37] A. Kierkegaard, S. Allam, G. Efraimsson, M. Åbom, Simulations of whistling and the whistling potentiality of an in-duct orifice with linear aeroacoustics, J. Sound Vib. 331 (5) (2012) 1084–1096, http://dx.doi.org/10.1016/j.jsv.2011.10.028.
[38] D. Fabre, R. Longobardi, V. Citro, P. Luchini, Acoustic impedance and hydrodynamic instability of the flow through a circular aperture in a thick plate, J. Fluid Mech. 885 (2020) http://dx.doi.org/10.1017/jfm.2019.953.
[39] S. Kottapalli, A. Hirschberg, N. Waterson, D. Smeulders, G. Nakiboglu, Singing and silent hydrodynamic modes in broadband orifice noise of a water pipe flow, 2022, private communication with A. Hirschberg.
[40] B. Gustavsen, A. Semlyen, Rational approximation of frequency domain responses by vector fitting, IEEE Trans. Power Del. 14 (3) (1999) 1052–1061, http://dx.doi.org/10.1109/61.772353.
[41] S.M. Gopinathan, D. Iurashev, A. Bigongiari, M. Heckl, Nonlinear analytical flame models with amplitude-dependent time-lag distributions, Int. J. Spray Combust. Dyn. 10 (4) (2018) 264–276, http://dx.doi.org/10.1177/1756827717728056.